Applied Catalysis B: Environment and Energy 351 (2024) 123975

Contents lists available at ScienceDirect

Applied Catalysis B: Environment and Energy

journal homepage: www.elsevier.com/locate/apcatb

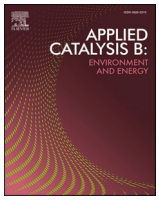

Deciphering the improvement in (H_2-)C_3H_6-SCR performance of Ag/Al_2O_3 catalysts prepared from warm-water-treated alumina: A NMR-assisted identification of the Ag anchoring sites of the alumina support

Yannick Millot [a,*,1], Guylène Costentin [a,2], Clémence Rodigue [a,b], Thomas Onfroy [a,3], Cyril Thomas [a,*,4]

[a] Sorbonne Université, CNRS, Laboratoire Réactivité de Surface, LRS, Paris 75005, France
[b] CESI, 93 boulevard de la Seine, Nanterre 92000, France

ARTICLE INFO

Keywords:
Catalysis
Ag/Al_2O_3
NO_x-TPD
FTIR
Selective Catalytic Reduction by Propene

ABSTRACT

Lean exhausts aftertreatment has been the subject of numerous investigations due to ever stringent regulations on pollutants emissions such as that of NO_x. Among aftertreatment technologies, the selective catalytic reduction of NO_x by the hydrocarbons (HC-SCR) has been studied intensively, in particular by using Ag/Al_2O_3 materials. The present work highlights that pretreatment of pristine Al_2O_3 in warm water prior to Ag deposition allows to prepare catalysts of significantly higher (H_2-)C_3H_6-SCR performance compared to conventional Ag/Al_2O_3 catalysts. In addition, NO_x-TPD-C_3H_6-SCR structure-activity correlations indicate that optimum composition of the Ag/Al_2O_3 catalysts can be improved by about 50% in terms of Ag content for the first time. Unprecedented in-depth NMR investigations allow for the identification of the alumina sites of importance in the anchoring of Ag. These sites are μ^1-OH groups located near the $(100)/(110)_l$ edge and then near the $(110)_b/(100)$ edge of Al_2O_3 crystallites and bonded to octahedrally coordinated Al species.

1. Introduction

Air pollution has become a growing health concern for human being [1] since the industrial revolution in the nineteen's century. Air quality is daily monitored worldwide [2] and the European Union acted on a reduction of certain atmospheric pollutants such as Sulfur dioxide (SO_2), Nitrogen oxides (NO_2 and NO), Non-Methane Volatil Organic Compounds (NMCOV), Ammonia (NH_3) and Particle Matter (PM) through the National Emission Ceilings Directive (NECD) [3]. While SO_2 emissions have been decreased by more than 80% from 1990 to 2011, mainly by using low sulfur content fuels [4], those of NO_x have decreased by only about 60% on a much longer period of time (from 1990 to 2017–2021) [5,6]. The reasons for this lower decrease in these latter atmospheric pollutants lie both on the fact that NO_x species are essentially formed by recombination of N_2 and O_2 in the flames of the combustion chambers, which can be hardly avoided unless by improving the combustion processes to a certain limit, and that transport is a significant contributor to NO_x emissions [7]. The mitigation of the NO_x emissions from light and heavy duty vehicles (LDVs and HDVs, respectively) has been achieved by the implementation of catalytic converters in Europe in 1977 for LDVs and 1988 for HDVs [7]. Whereas Three-Way Catalysts (TWC) have been shown to be very efficient in the concomitant remediation of CO, unburnt hydrocarbons and NO_x from stoichiometric exhausts of gasoline engines [8], such catalytic devices have been found to be unsuccessful in the reduction of NO_x from lean exhausts of gasoline and diesel engines [9]. As stated by Burch, promoting a reduction reaction, such as that of NO_x reduction to N_2, in a strongly oxidizing environment, namely lean mixtures, appears to be extremely challenging from a chemistry viewpoint [9]. To overcome such a difficulty, the use of catalysts using ammonia as a reductant (NH_3-SCR) [10,11]

* Correspondence to: Sorbonne Université, CNRS, Laboratoire Réactivité de Surface, LRS, UMR CNRS 7197, 4 Place Jussieu, Tour 43-53, 3ème étage, Case 178, Paris 75252, France.
E-mail addresses: yannick.millot@sorbonne-universite.fr (Y. Millot), cyril.thomas@sorbonne-universite.fr (C. Thomas).
[1] orcid.org/0009-0005-1044-6369
[2] orcid.org/0000-0003-1559-6890
[3] orcid.org/0009-0006-1621-4566
[4] orcid.org/ 0000-0003-4224-6095

https://doi.org/10.1016/j.apcatb.2024.123975
Received 8 February 2024; Received in revised form 13 March 2024; Accepted 17 March 2024
Available online 20 March 2024

and Lean NO_x Trap (LNT) [12] have been developed to catalyze the reduction of NO_x to N_2 in lean exhausts. Yet the ammonia slip in NH_3-SCR, an atmospheric regulated pollutant [3], and CO_2 penalties, due to the short incursions in rich mixtures needed to proceed to the reduction of the NO_x adsorbed species [12], are inherent drawbacks of these aftertreatment technologies [13] from air pollution and global warming viewpoints.

Many studies have been devoted to the selective catalytic reduction of NO_x by Hydrocarbons (HC-SCR) [9,14,15], as an elegant potential alternative of the NH_3-SCR and LNT technologies [9], since the pioneering remarkable discoveries of the Ag/Al_2O_3 catalyst for C_3H_6-SCR by Miyadera [16] and for low-temperature promoting effect H_2 in H_2-C_{1-4}-SCR by Satokawa and co-workers [17,18]. Not only light hydrocarbons have been reported to be efficient reductants of NO_x over Ag/Al_2O_3, either in the presence or in the absence of H_2, but also long chain alkanes [9,14,19–22] and alcohols [9,14,23–26], or a mixture of both [27]. Overall, the studies performed to date have essentially concluded to the elevated dispersion of Ag on Al_2O_3 and that oxidized Ag species, such as electron-deficient clusters ($Ag_n^{\delta+}$) [28,29], would be the active catalytic species [9,15,30]. In HC-SCR, the formation of N_2 would result from the interaction of NO_x, either in an adsorbed state [30] or not, with the hydrocarbons to form various intermediates [15, 31], for which isocyanates have been claimed to be among the most important intermediates leading ultimately to nitrogen [32–35]. It has also been reported that the best catalytic performance in HC-SCR was obtained with an optimum loading of 2 wt% Ag on alumina [16,30, 36–39] and that such an optimum Ag loading would also stand for H_2-promoted HC-SCR [21,28]. Based upon a disruptive approach, namely the challenging characterization of the alumina support of the Ag/Al_2O_3 catalysts by adsorption-desorption of NO_x (NO_x-TPD method) developed initially for tungstated-zirconia materials [40,41], NO_x-TPD-(H_2-)C_3H_6-SCR structure-activity relationships led some of us to conclude that (i) the optimum Ag loading of 2 wt% could be attributed to the maximum content of Ag for which this metal remained in a highly-dispersed state on Al_2O_3 [42] and (ii) that this optimum loading did not stand for H_2-C_3H_6-SCR as the reduction of NO_x to N_2 was found to be favored as the Ag loading decreased [43]. Earlier literature reports attributed the H_2 promoting effect to (i) changes in the speciation of the Ag species [21,28,34,44], (ii) enhancement of hydrocarbon activation to surface oxygenated compounds [22,28,34,45], (iii) the formation of reactive oxygen species such as peroxides [28,34,46], (iv) changes in the surface concentration of NO_x adsorbed species [34,44,45,47,48], and/or (v) the modification of chemical reactions [9,49,50]. In addition, Burch and co-workers have claimed that the formation of organo-NO_x intermediates, resulting from the interaction of NO_x and activated hydrocarbons species, would be rate determining for both HC-SCR [15] and H_2-HC-SCR [51]. In the case of HC-SCR, Thomas and co-workers reported that the temperature at which NO_x adsorbed species interacted with hydrocarbons may be valuably monitored by exposing pre-adsorbed NO_x species to hydrocarbon-containing feeds under temperature-transient conditions [52,53]. By using a similar approach with C_3H_6-containing feeds of increasing complexity, Thomas suggested that H_2 could also promote the formation-decomposition-reaction of organo-NO_x species at the lowest temperatures based on the temperature-transient reactivity of preadsorbed nitrates [54].

Despite the tremendous number of investigations performed in this particular field to date, the limited activity of the Ag/Al_2O_3 catalysts over the temperature of interest of the catalytic converters prevented their implementation [55], as exhausts temperatures as low as 150 °C are commonly met in these devices [56]. Hence many works have been devoted to the modification of the silver alumina system by promoters. For instance, the addition of limited amounts of chlorides has been claimed recently to promote (H_2-)C_3H_6-SCR mainly at high Ag loadings because of the stabilization of electron-deficient Ag clusters ($Ag_n^{\delta+}$) in greater proportion compared to that in the Cl-free catalyst [57]. Likewise, the introduction of tungstates on Al_2O_3 has been reported to promote C_2H_5OH-SCR [58]. Such a promotional effect of tungstates for the Ag/Al_2O_3 system contrasts with the detrimental effect of tungstates that one of us observed on n-C_{10}-SCR [59], however, which led us to confirm the importance of the close proximity between the silver species and the alumina carrier. The importance of Al_2O_3 as a supporting oxide of Ag for H_2-HC-SCR, - as deduced from the lack of reactivity of Ag/SiO_2, Ag/TiO_2 and Ag/ZrO_2 for H_2-C_3H_8-SCR [18] and also indicated by the positive reaction order with respect NO up to a silver loading of about 2 wt% on Al_2O_3 in H_2-C_3H_6-SCR [43] -, therefore makes the promotion of Ag/Al_2O_3 extremely risky as the introduced promoters may also compete with the alumina sites involved in H_2-HC-SCR. Several studies have aimed at investigating the influence of the nature of Al_2O_3 via the use of its precursors [60,61] or its morphology [62–64]. The claim of Yang et al. regarding the higher catalytic C_3H_8-SCR performance of a silver alumina sample prepared from Al_2O_3 with a flake morphology compared to that prepared with a sphere morphology must be taken with caution, however, as the synthesis of the latter support included sulfates, whereas such anions were not used in the synthesis of Al_2O_3--flake [64]. Not only the presence of sulphates on Al_2O_3 has been shown to be detrimental to the NO_x adsorption capacity [64,65] but also to C_3H_8-SCR performance [65]. Several studies have also reported on the use of newly developed synthesis methods to improve the efficiency of the silver alumina catalysts in (H_2-)HC-SCR. Petitto and Delahaye reported that the heating of a mechanical mixture made of Ag_2O and Al_2O_3 in a wet atmosphere above 600 °C led to more active catalysts in n-C_{10}-SCR compared to those prepared conventionally by impregnation of alumina by a silver nitrate aqueous solution [66]. This peculiarity may be linked to the agglomeration/oxidative dispersion of Ag nanoparticles in the presence of a wet oxidizing atmosphere at high temperature [67] and the importance of the surface hydroxyls of γ-Al_2O_3 for such processes [68]. The use of silver alumina catalysts prepared by ball milling have also showed promising n-C_8-SCR at temperature much lower than those usually reported in the field over samples prepared conventionally [69], whereas such a beneficial effect of ball milling could not be observed in C_2H_5OH-SCR [70]. Yet it must be highlighted that the speed with which the ball-milled samples were prepared has been reported to be critical in making efficient Ag/Al_2O_3 catalysts, as the use of high-speed ball milling appeared to be detrimental to SCR reactions [71]. The greater effectiveness of ball-milled-prepared silver alumina catalysts compared to conventionally prepared samples has also been illustrated in H_2-n-C_8-SCR and assigned to modifications in the affinity of water and hydrocarbons with the Al_2O_3 surface [51] and the concentration/rate of formation of isocyanate intermediates [51,71]. Hence these latter studies have prompted on the importance of the Al_2O_3 supporting oxide for the SCR reactions. Recently, it has been elegantly shown that Ag dispersion capacity, *i.e.* the amount of Ag anchored onto Al_2O_3 in a highly dispersed state, was strongly correlated to the surface OH content of such a supporting oxide [68]. In an earlier study, Thomas and co-workers have reported that H_2-C_3H_6-SCR could be increased drastically over an alumina support that was pretreated in warm water prior to deposition of Ag by conventional impregnation [72]. Such a peculiarity was inferred to the preferential anchoring of Ag on OH groups that were not present in the pristine Al_2O_3 support, but created during its treatment in warm water, and hence the preservation of a higher NO_x coverage [43] in the warm-water-treated-Al_2O_3-supported Ag sample compared to the conventionally prepared Ag/Al_2O_3 catalyst [72]. To our knowledge, enhanced hydroxylation of Al_2O_3 to favor metal anchoring has been reported scarcely in the case of supported Pt catalysts [73,74] only.

Whereas NMR [61,63,64,70,75,76] and FTIR [63,75–77] spectroscopies are known to be powerful techniques to monitor protons from the OH groups and/or the Al species of Al_2O_3, very few investigations have been reported on their use to monitor the changes brought about by the introduction of Ag on Al_2O_3. 1D ^1H [63,70] and ^{27}Al [61,63,64,75,76] NMR have been essentially used to characterize Ag/γ-Al_2O_3 samples, whereas in-depth characterization of γ-alumina has been provided

rather recently with 2D ^{1}H–^{1}H DQ [78–81] and ^{1}H–^{27}Al D-HMQC [78–82] sequences.

Firstly, the present work aims at providing further insights into the influence of a modification of γ-Al_2O_3 in warm water prior to deposition of Ag, following a procedure similar to that reported earlier [72] but over a series of Ag/γ-Al_2O_3 catalysts with Ag loadings varying from about 1 to 9 wt%, on the catalytic performance in C_3H_6-SCR promoted or not by hydrogen ((H_2-)C_3H_6-SCR) so as to establish NO_x-TPD-(H_2-)C_3H_6-SCR structure-activity correlations. Secondly, FTIR and NMR spectroscopic investigations are performed on this series of Ag/γ-Al_2O_3 catalysts to unravel the preferential Ag anchoring sites of γ-Al_2O_3, which would pave the way to the design of alumina supports of improved efficiency not only in the dispersion of Ag species of interest in the C_3H_6-SCR field but also for the deposition of any other transition metals on such a widely used supporting oxide.

2. Experimental

2.1. Catalyst preparation

As indicated in earlier literature reports, Ag/Al_2O_3 catalysts are most often prepared by incipient wetness impregnation of the alumina support by an aqueous solution of $AgNO_3$ [42,43]. In the present work, a series of Ag/Al_2O_3-H_2O samples was prepared by incipient wetness impregnation after the γ-Al_2O_3 support (Procatalyse, 125–200 μm, 40 g) had been treated in 400 mL of warm water (80 °C) for 66 h without any stirring. After filtering and drying under vacuum for 16 h at RT, such a warm-water-treated alumina support was calcined at 600 °C (3 °C/min heating rate from RT to 600 °C) for 4 h. The as-modified support, denoted as Al_2O_3-H_2O, was used to prepare the Ag(x)/Al_2O_3-H_2O series of samples, where x denotes the Ag content (wt%), determined by ICP-OES, that was deposited on Al_2O_3-H_2O by incipient wetness impregnation of aqueous solutions of $AgNO_3$. After ageing under vacuum at RT for 4 h, the samples were dried at 100 °C for 18 h in a laboratory oven. Finally, the Ag(x)/Al_2O_3-H_2O samples were calcined at 600 °C (3 °C/min heating rate from RT to 600 °C) for 4 h. This procedure appears to differ substantially from that reported in our earlier study in which the γ-Al_2O_3 support was vigorously stirred in warm water (80 °C) for 24 h, which resulted in the loss of most of the 125–200 μm fraction due to severe attrition of the grains, and for which Ag was deposited on a vacuum-dried (not calcined) Al_2O_3-OH support [72]. For comparison, where necessary, Ag(x)/Al_2O_3 samples were also prepared following the procedure described earlier [42,43], namely incipient wetness impregnation of pristine γ-Al_2O_3 by aqueous $AgNO_3$ solutions. Figure S1 provides a schematic summary of the synthesis conditions used for both series of silver alumina samples.

2.2. Catalyst characterization

Ag loadings were determined by ICP-OES (CREALINS, Lyon).

XRD patterns of Al_2O_3-H_2O (vacuum-dried for 16 h and calcined at 600 °C for 4 h) were recorded in the 2θ range of 10−90° with 0.01° steps and 0.5 s/step with a Bruker D8 ADVANCE diffractometer equipped with a copper source (λCu-Kα1 = 1.54056 Å and λCu-Kα2 = 1.54439 Å) and a LynxEye detector.

N_2-sorption measurements were carried out on a Belsorp MAX Instrument (Bel Japan) at 77 K after evacuation of the samples at 300 °C for 3 h. The specific surface area of the samples was determined by using the BET method in the $0.05 < p / p^0 < 0.30$ domain.

SEM-FEG imaging of the supporting oxides was done with a Hitachi SU-70 field emission gun scanning electron microscope at magnifications varying from × 300 to × 10,000. The 125–200 μm powder samples were deposited as is onto carbon adhesives taped on an aluminum SEM support. Imaging was performed without any metallization at 1 kV and a working distance of about 15 mm, hence by an "in lens" secondary electron detector (SE-Upper).

NO_x Temperature-Programmed Desorption (NO_x-TPD) experiments were carried out in a U-type quartz reactor (12 mm i.d.). The samples (about 0.200 g) were held on a plug of quartz wool and the temperature was set by a Eurotherm 2408 temperature controller using a K-type thermocouple. Reactant gases (Air Liquide) were used as received and fed from independent gas cylinders by means of mass flow controllers (Brooks 5850TR) with a total flow rate of 230 mL_{NTP}/min. Prior to the NO_x-TPD experiments, the samples were calcined at 500 °C (3 °C/min) for 2 h under a flow rate of 100 mL_{NTP}/min of 20% O_2/He. The reactor outlet was continuously monitored by a chemiluminescence NO_x analyzer (Thermo Environmental Instruments 42C-HL) that allowed the simultaneous detection of both NO and NO_2. The samples were exposed to the adsorption mixture (Typically 385 ppm NO_x and 8% O_2 in He with a total flow rate of 230 mL_{NTP}/min) for 4 h at RT. This latter parameter was set to ensure that saturation coverage was reached for all of the samples investigated under the present experimental conditions, as the time after which no change was observed in the gas phase NO_x concentrations was found to be dependent on the Ag loadings of the silver alumina samples. Before NO_x-TPD, the samples were flushed under a flow of 230 mL_{NTP}/min of O_2 8%/He at RT for about 1 h to remove weakly chemisorbed species until the NO and NO_2 concentrations detected at the outlet of the reactor were found to be negligible. NO_x-TPD experiments were carried out from RT to 500 °C at a heating rate of 3 °C/min under a flow of 230 mL_{NTP}/min of O_2 8%/He.

FTIR spectra of the Ag/γ-Al_2O_3 samples were collected in transmission mode on a Bruker Vertex 70 FTIR spectrometer equipped with a liquid N_2-cooled MCT detector and a data acquisition station. 64 scans were averaged with a spectral resolution of 4 cm^{-1}. The samples were pressed into self-supporting wafers of 6–8 mg/cm^2 (12–16 mg for wafers of 1.6 cm diameter). The wafers were loaded into a moveable glass sample holder, equipped on top with an iron magnet, and inserted in a conventional quartz glass cell (CaF_2 windows) connected to a vacuum system. The iron magnet allowed for the transfer of the catalyst sample from the oven-heated region to the infrared light beam. Before spectrum recording, the catalysts were submitted to a dynamic (20 mL/min) oxidizing pretreatment (O_2, Air Liquide, 99.999%) at 500 °C for 2 h at atmospheric pressure. The samples were then evacuated (5×10^{-6} mbar) at 400 °C for 1 h. Finally, the temperature was decreased to RT under dynamic vacuum.

Magnetic Resonance (MAS NMR) spectra were recorded at room temperature using a Bruker Advance spectrometer operating in a static field of 11.7 T. The resonance frequency of ^{1}H and ^{27}Al were 500.2 and 130.3 MHz, respectively. A Bruker 4 mm MAS probe was used to perform the experiments at a spinning speed of 14 kHz for one-dimensional (1D) spectra and 12.5 kHz for two-dimensional (2D) spectra. The ^{1}H and ^{27}Al chemical shifts were referenced to external standards of tetra-methylsilane (TMS) and $Al(NO_3)_3$ aqueous solutions, respectively. For all experiments, the powdered samples were first calcined at 500 °C (3 C/min) for 2 h under 100 mL_{NTP}/min of O_2(20%)/He using a quartz reactor equipped with stop valves. The samples were then flushed with 100 mL_{NTP}/min of He for 15 min at RT before closing of the valves of the reactor to prevent the samples from exposure to ambient atmosphere and potential rehydration. Selected samples (Al_2O_3-H_2O and Ag(1)/Al_2O_3-H_2O), were also contacted with NO_x (96% NO + 4% NO_2) by flowing a NO_x(385 ppm)-O_2(8%)-He mixture at RT and 230 mL_{NTP}/min for 4 h before being flushed by He (100 mL_{NTP}/min) for 1 h. Samples were then transferred from the reactor to the NMR rotors into a glovebox where the NMR rotors were finally closed. ^{1}H MAS NMR 1D spectra were recorded with a 90° pulse duration of 2.75 μs, a recycle delay of 10 s, and a scan number of 64. The MAS equipment for rotation was carefully cleaned with ethanol before being dried to avoid spurious proton signals. From two successive experiments performed with the same recording conditions and using the same empty or filled rotor, the signals of the probe and the rotor were subtracted from the total FID. The ^{1}H DQ-SQ 2D spectrum was recorded with the POST-C7 sequence for excitation and conversion block, and a RF field strength

was used during the dipolar recoupling sequence of 87.5 kHz and 60 t1 increments of 80 μs for F1 dimension acquisition. The ^{27}Al-^{1}H D-HMQC (heteronuclear multiple quantum coherence) experiments were performed with RF nutation frequencies of 9 and 92 kHz for ^{27}Al and ^{1}H, respectively. A $SR4_1^2$ method was used as the recoupling sequence to reintroduce ^{27}Al-^{1}H dipolar interaction with a RF field strength of 25 kHz (=2*νrot) during 960 μs. The recorded spectra result from averaging 4096 transients and a recycle delay of 0.5 s.

2.3. (H_2-)C_3H_6-SCR catalytic experiments

Steady state catalytic (H_2-)C_3H_6-SCR experiments were carried out in a U-type quartz reactor (12 mm i.d.). In contrast to most studies reported to date, the amount of silver introduced in the catalyst beds remained essentially constant when the silver loading of the Ag(x)/Al_2O_3-H_2O samples varied. To be compared to the catalytic data recorded earlier on silver alumina samples prepared with a non-treated Al_2O_3 support [42,43], the samples were held on plugs of quartz wool and consisted in about 0.38 g of mechanical mixtures of Ag(x)/Al_2O_3-H_2O and Al_2O_3 of the same grain sizes in which the amount of Ag was equal to 30.9 ± 0.1 μmol. The temperature of the tubular furnace was set by a Eurotherm 2408 temperature controller using a K type thermocouple. Prior to the (H_2-)C_3H_6-SCR experiments, the samples were calcined in situ in O_2(20%)–He at 550 °C (3 °C/min) for 2 h with a flow rate of 100 mL_{NTP}/min. After cooling down to 150 °C, the samples were submitted to a C_3H_6-SCR experiment from 150 to 550 °C [42]. The samples were subsequently exposed to the H_2-C_3H_6-SCR feed at 150° C [43]. H_2(2%/He), NO(4000 ppm/He), C_3H_6(2000 ppm/He), O_2(100%) and He (100%) were fed from independent cylinders (Air Liquide) without any further purification via mass flow controllers (Brooks 5850TR). The composition of the H_2-NO_x-C_3H_6-O_2-He feeds was: 0 or 0.21% H_2, 385 ppm NO_x(~96% NO), 400 ppm C_3H_6 and 8% O_2 in He, and the total flow rate was 230 mL_{NTP}/min. The temperature was then increased stepwise from 150 to 550 °C with 25 °C increments and left for about 1 h at each temperature step. The reactor outflow was analyzed using a μ-GC (Agilent Technologies, CP4900) equipped with two channels. The first channel, a 5Amolecular sieve column (80 °C, 150 kPa He, 200 ms injection time, 37 s backflush time), was used to separate H_2, N_2, O_2 and CO, while the second channel, equipped with a poraplot Q column (60 °C, 150 kPa He, 200 ms injection time), was used to separate CO_2, N_2O, C_3H_6 and H_2O. A chemiluminescence NO_x analyzer (Thermo Environmental Instruments 42C-HL) allowed the simultaneous detection of both NO and NO_2. NO_x conversions to N_2 and N_2O were calculated as follows:

$$X_{NOx\ to\ N2}\ (\%) = (2 \times [N_2])/[NO_x]_{inlet}) \times 100, \quad (1)$$

$$X_{NOx\ to\ N2O}\ (\%) = (2 \times [N_2O])/[NO_x]_{inlet}) \times 100, \quad (2)$$

where $[NO_x]_{inlet}$, $[N_2]$ and $[N_2O]$ were the concentrations in NO_x measured at the inlet of the reactor and in N_2 and N_2O at the outlet of the reactor, respectively. C_3H_6 conversions were calculated on the basis of the CO_x (CO + CO_2) products formed:

$$X_{C3H6}\ (\%) = ([CO] + [CO_2])/([C_3H_6]_{inlet} \times 3) \times 100, \quad (3)$$

where [CO], $[CO_2]$ and $[C_3H_6]_{inlet}$ were the concentrations of CO and CO_2 measured at the outlet of the reactor and that of C_3H_6 measured at the inlet of the reactor, respectively. The comparison of the catalytic performances of the materials investigated in the present study was also made on the basis of an efficiency criterion (%) in the reduction of NO_x to N_2 in the 150–550 °C range of temperatures. This criterion compares the catalytic performance of the investigated samples to those of a catalyst that would allow for the full reduction of NO_x to N_2 from 150 to 550 °C (100% efficiency).

3. Results

3.1. Influence of a pretreatment of Al_2O_3 in warm water on the structural and textural properties of the Ag/Al_2O_3 materials

The Ag contents and the surface areas of the samples prepared in the present work are listed in Table 1. It can be first seen that exposure of the pristine Al_2O_3 support to water at 80 °C for 66 h with subsequent drying and calcination at 600 °C for 4 h led to a slight increase in its surface area (Al_2O_3-H_2O ~ 195 m^2/g) compared to the starting material (Al_2O_3 ~ 180 m^2/g). It must be noted that a similar surface area (195 m^2/g) was also measured on dried Al_2O_3-H_2O, which indicates that the increase in surface area of this sample cannot be attributed to the calcination step. In an earlier study in which the same pristine Al_2O_3 support was exposed to water at 80 °C but for a much shorter duration, *i.e.* 24 h [72] compared to 66 h in the present work, the limited increase in specific area of Al_2O_3-OH (185 m^2/g) compared to untreated Al_2O_3 (180 m^2/g) [72] did not appear to be significant at first sight. From the present surface area data, it can be concluded that the increase in surface area was indeed significant in the earlier work [72], albeit very limited (+ 5 m^2/g), however, as the increase in surface area measured in the present work (+ 15 m^2/g) appears to be roughly proportional to the duration of the exposure of Al_2O_3 to water at 80 °C (from 24 h [72] to 66 h in the present work), as also reported previously by Lefèvre et al. [83]. It can be observed that the measured Ag contents are in good agreement with those targeted. Overall, the specific surface area per g of sample decreases as the Ag content increases and the associated surface area per g of Al_2O_3 remains essentially constant (Table 1).

As reported earlier [72,84], the treatment of γ-Al_2O_3 in warm water led to the formation of bayerite crystallites in the Al_2O_3-H_2O sample dried at RT under vacuum for 16 h [72], as indicated by the reflections at 18.8, 20.3, 27.9, 40.6, 53.2, 63.8, 70.8 and 78.9° (Figure S2, ● on

Table 1
Ag contents determined by ICP-OES and surface areas of the newly prepared silver alumina samples.

Samples	Targeted Ag content (wt%)	Measured Ag content (wt%)	Surface area (m^2/g)	Surface area (m^2/g_{Al2O3})
Al_2O_3-H_2O	-	-	195	195
Ag(1)/Al_2O_3-H_2O	1.00	1.11	192	194
Ag(2)/Al_2O_3-H_2O	2.00	2.18	184	189
Ag(3)/Al_2O_3-H_2O	3.00	3.23	187	193
Ag(5)/Al_2O_3-H_2O	5.00	5.11	181	191
Ag(7)/Al_2O_3-H_2O	7.00	7.13	179	193
Ag(9)/Al_2O_3-H_2O	9.00	9.21	172	189
Al_2O_3	-	-	180	180
Ag(1)/Al_2O_3	1.00	1.05	178	180
Ag(2)/Al_2O_3	2.00	2.12	176	180
Ag(3)/Al_2O_3	3.00	3.15	173	179
Ag(4)/Al_2O_3	4.00	4.19	171	178
Ag(7)/Al_2O_3	7.00	-	167	180[1]

[*] Surface area estimated on the basis of a theoretical Ag loading of 7 wt%.

green trace). The longer exposure of the pristine Al_2O_3 support in water at 80 °C in the present work (66 h) compared to that in our earlier work (24 h [72]) did not seem to have a significant influence on the formed bayerite crystallites, as the (201) bayerite to (400) Al_2O_3 intensity ratio of the peaks at 40.6 and 46.0° appears to be similar in both XRD patterns (1.29 in Figure S2 compared to 1.26 in Fig. 3 of ref. [72]). Yet, the longer exposure to the pristine Al_2O_3 support to water at 80 °C induced the formation of gibbsite, as indicated by a diffraction peak of low intensity at 18.3° (Figure S2), which could hardly be observed earlier in the tail of the bayerite peak at 18.8° [72]. As both bayerite and gibbsite can transform subsequently to boehmite and γ-Al_2O_3 upon heating and/or η- and χ-Al_2O_3 transition aluminas [85], which can be hardly distinguished from γ-Al_2O_3 by XRD, the XRD pattern after calcination of Al_2O_3 pretreated in warm water (Figure S2, blue trace) therefore closely resembles that of the pristine γ-Al_2O_3 support [72]. If any surface modifications of the pristine Al_2O_3 support had been achieved by its exposure to water at 80 °C, these changes can hardly be monitored by XRD, in agreement with the inherent bulk sensitivity of such a technique.

Representative SEM images of the pristine Al_2O_3 support, and the dried and calcined warm-water-pretreated Al_2O_3 samples are displayed in Figure S3. Figure S3 shows that the surface of the grains of the pristine Al_2O_3 support are rather smooth (a,b) and the presence of small entities of ill-defined shape at elevated magnification (c). The pretreatment of Al_2O_3 in water at 80 °C for 66 h had a dramatic influence on the Al_2O_3 grains that became almost fully covered by crystallites (Figure S3d) exhibiting a platelet-like morphology (Figure S3e,f) with a wideness as high as 2–3 μm. The fact that the platelets of the present work were found to be bigger than those observed earlier by Lefèvre et al. [83] can be assigned to the much higher temperature at which Al_2O_3 was immersed in water compared to that in the earlier study of Lefèvre et al. [83], and a corresponding improvement in the kinetics of dissolution-reprecipitation of Al_2O_3 as bayerite [84]. The presence of such well-crystallized platelets after treatment of Al_2O_3 in water is consistent with the appearance of the thin XRD contributions observed in the corresponding pattern (Figure S2, green trace). Figure S3g-i shows that the peculiar morphology observed in dried warm-water-pretreated Al_2O_3 (Figure S3d-f) was preserved after calcination (Al_2O_3-H_2O). The presence of such micrometric Al_2O_3 platelets (disappearance of the bayerite diffraction peaks on the blue diffraction pattern in Figure S2) onto the surface of the Al_2O_3 grains should be increasing the roughness of the external surface of the Al_2O_3-H_2O grains and should be at the origin of the moderate, but significant, increase in the surface area of Al_2O_3-H_2O compared to Al_2O_3 (Table 1).

3.2. *Influence of a pretreatment of Al_2O_3 in warm water and the deposition of Ag on surface hydroxyl groups*

Characterization of the surface OH groups of Al_2O_3 was performed by FTIR. Figure S4a shows that pretreatment of Al_2O_3 in water at 80 °C led to changes in the absorption spectrum in the region of the hydroxyl groups. Overall the envelope of the hydroxyl groups (3800–3400 cm^{-1}) increased by about 10% in Al_2O_3-H_2O compared to Al_2O_3 and the intensity of the contributions at 3790 and 3754 cm^{-1} decreased, whereas those at 3770, 3680 3633 and 3602 cm^{-1} increased and that at 3730 cm^{-1} remained essentially constant in Al_2O_3-H_2O compared to Al_2O_3. The introduction of increasing amount of Ag on Al_2O_3-H_2O led to a vanishing of the bands at 3790 and 3754 cm^{-1} at the lowest content of Ag, a pronounced decrease of the bands at 3770 and 3680 cm^{-1} for Ag (1)/Al_2O_3-H_2O followed by a more moderate decrease at higher Ag loadings and an increase in that at 3730 cm^{-1} up to Ag(3)/Al_2O_3-H_2O before decreasing at a higher Ag loading (Figure S4b). Such trends are in agreement with those reported earlier on Ag(*x*)/Al_2O_3 samples [63,75,77,80]. The nature of the corresponding OH groups of Al_2O_3 has been debated comprehensively [63,75,77,80,86–88] and will be discussed in relation with other findings in Section 4.2.

Before describing the NMR data, it must be recalled that the various hydroxyl groups (OH) of γ-alumina are commonly denoted as μ^n-OH, which denotes that the hydroxyl group is bounded to *n* aluminum atoms [78]. The ^{1}H spectrum of γ-Al_2O_3 (Fig. 1, spectrum a) can be decomposed into three regions between (i) –1 and 1 ppm and (ii) 1 and 3 ppm, and (iii) for a chemical shift greater than 3 ppm. In earlier literature reports, the first region has been attributed to terminal hydroxyl groups (μ^1-OH), the second one to doubly-bridging hydroxyl groups (μ^2-OH) and the last one to triply-bridging hydroxyl groups (μ^3-OH) and residual water [78]. More recently, thanks to DFT calculations, a new assignment of the ^{1}H chemical shifts has been proposed [81]. The first region corresponds to μ^1-OH species located on the edges of the γ-Al_2O_3 crystallites, while the second region corresponds to μ^1-OH and μ^2-OH species located essentially on the Al_2O_3 facets. Finally, the ^{1}H contributions with a chemical shift greater than 3 ppm were assigned to μ^1-OH, μ^2-OH and μ^3-OH species with H-bond donors. The effect of the pretreatment of Al_2O_3 in warm water on its hydroxylation can be seen in Fig. 1 (spectra a and b). The integral of the Al_2O_3-H_2O spectrum (Fig. 1, spectrum b) is about 1.6 times greater than that of the Al_2O_3 spectrum (Fig. 1, spectrum

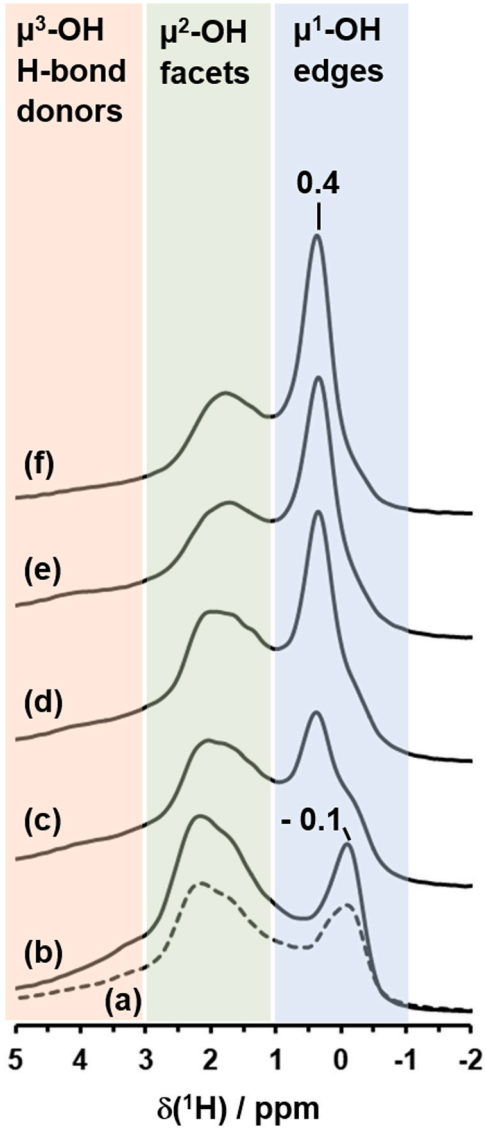

Fig. 1. ^{1}H MAS NMR spectra of (a) Al_2O_3 (dotted line), (b) Al_2O_3-H_2O, (c) Ag (1)/Al_2O_3-H_2O, (d), Ag(2)/Al_2O_3-H_2O, (e) Ag(3)/Al_2O_3-H_2O and (f) Ag(5)/Al_2O_3-H_2O. Signal assignment based on the earlier studies of Taoufik et al. [78] and Batista et al. [81].

a), hence showing a significant increase in the amount of protons present on the alumina surface after pretreatment in warm water.

2D double quantum-single quantum (DQSQ) correlation experiment provides useful information on the proximities (< ~ 5 Å) between dipolar-coupled protons, as the observed DQ coherences depend strongly on the internuclear distance. The diagonal peaks (δA, 2δA) are autocorrelation peaks resulting from the dipolar interaction of spins with identical chemical shift, while the pairs of off-diagonal peaks at (δA, δA+δB) and (δB, δA+δB) correspond to correlations between two spins with different chemical shifts. Usually, the intensity of these correlation peaks reflects the strength of the dipolar interaction between the spin pairs and therefore the distance between the different proton species. In agreement with the A-G OH terminology defined by Merle et al. [80] (Fig. 2), the ^{1}H–^{1}H DQSQ MAS NMR spectrum of Al_2O_3-H_2O (Fig. 3a) exhibits two autocorrelation peaks at – 0.10 and 2.25 ppm attributed to μ^1-OH (F) and μ^2-OH (G) species, respectively. Two off-diagonal correlations between μ^1-OH and μ^2-OH species are also observed, which show proximity of two μ^1-OH sites (– 0.15 ppm (C) and – 0.20 ppm (A)) with two μ^2-OH species (1.90 ppm (D) and 2.50 ppm (B)), respectively. In addition, an off diagonal correlation between two μ^2-OH species (1.90 ppm (D) and 1.55 ppm (E)) is visible. This experiment shows that the signal at about – 0.10 ppm (Fig. 1) assigned to μ^1-OH groups is composed of at least three different species with proton shifts at – 0.20 ppm (A), – 0.15 ppm (C) and – 0.1 ppm (F). The ^{1}H–^{1}H DQSQ MAS NMR spectrum and associated proximity information (Fig. 3a) are found to be identical to those reported by Merle et al. [80] and fairly close to those reported by Batista et al. [81] and Völker et al. [82]. The differences in the ^{1}H–^{1}H DQSQ MAS NMR spectrum and associated proximity information (Fig. 3a) with those of the latter studies may be due to differences in the morphology of the studied aluminas and/or sample pre-treatments. Finally, it should be also noted that the ^{1}H–^{1}H DQSQ MAS NMR spectrum seems to show a proximity between OH species with and without H-bond donors at about 3.50 ppm.

The presence of 1 wt% Ag on Al_2O_3-H_2O leads to an overall decrease in μ^2-OH species (1–3 ppm), an increase in the overall amount of μ^1-OH species (– 0.1 to + 1 ppm) and the shift of some of the μ^1-OH species (from about – 0.1 ppm to about 0.4 ppm) (Fig. 1, spectra b and c). Not only such trends have already been reported by Wang et al. [63] for Ag/Al_2O_3 but also, more surprisingly, by Barrow et al. for SrO/Al_2O_3 [89]. The ^{1}H–^{1}H DQSQ spectrum of $Ag(1)/Al_2O_3$-H_2O (Fig. 3b), which has not been reported to date to the best of our knowledge, provides additional information about the newly formed μ^1-OH species at about 0.4 ppm disturbed by the addition of Ag on Al_2O_3-H_2O. The comparison of Fig. 3b and Fig. 3a indicates that part of the – 0.20 ppm μ^1-OH (A) and most of the – 0.10 ppm μ^1-OH (F) species are shifted to 0.35 ppm (A') and 0.40 ppm (F') μ^1-OH species, respectively, on the addition of 1 wt% Ag on Al_2O_3-H_2O. The μ^1-OH (F') species are coupled with themselves as being located on the diagonal of the spectrum shown in Fig. 3b, whereas the μ^1-OH (A') species are coupled with μ^2-OH (B') species, which corresponds to μ^2-OH (B) species shifted to lower chemical shift (2.10 ppm instead of 2.50 ppm). In contrast, – 0.15 ppm μ^1-OH (C), 1.90 ppm μ^2-OH (D), 1.55 ppm μ^2-OH (E) and 2.25 ppm μ^2-OH (G) species do not appear to be affected by the presence of silver atoms (same chemical shift and same correlation in Fig. 3b compared to Fig. 3a). The sample containing 2 wt% silver shows hardly any change in chemical shifts of most of the protons, but only a slight decrease in the intensity of μ^2-OH (1–3 ppm and particularly at higher chemical shifts) and – 0.15 ppm

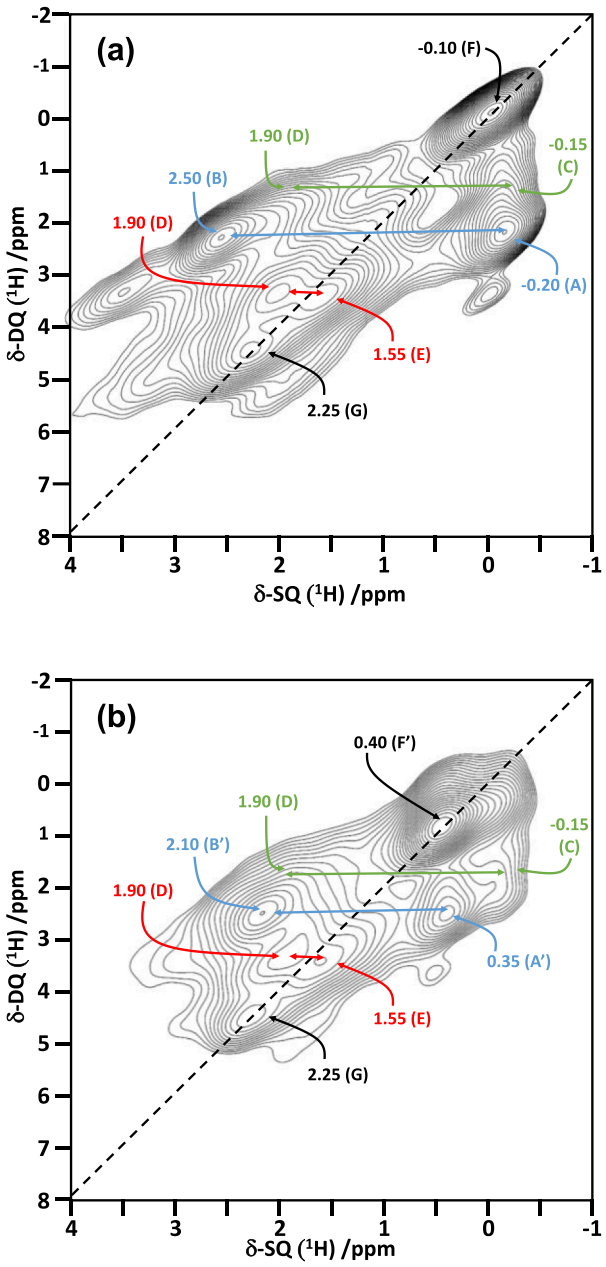

Fig. 3. ^{1}H–^{1}H DQSQ MAS NMR spectra of (a) Al_2O_3-H_2O and (b) $Ag(1)/Al_2O_3$-H_2O.

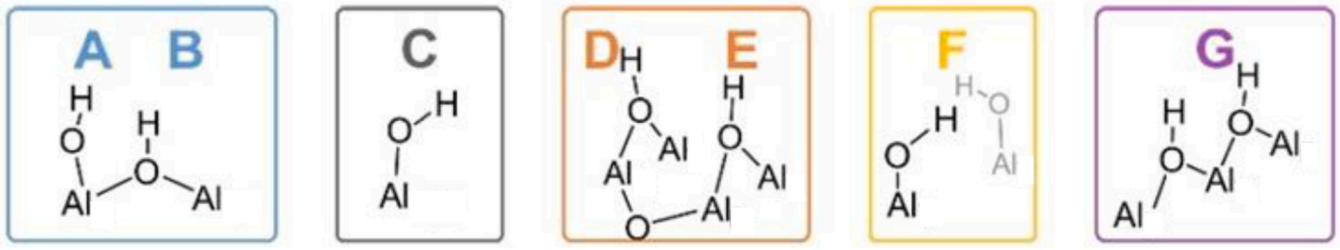

Fig. 2. Structure of the main hydroxyl groups of γ-Al_2O_3 adapted from the work of Merle et al. [80].

μ^1-OH (C) species, as well as an increase in intensity and a narrowing of the signals corresponding to μ^1-OH (A') and (F') species around 0.4 ppm (Fig. 1, spectrum d and Figure S5). For samples with 3 and 5 wt% silver on alumina (Fig. 1, spectra e and f), a disappearance of the μ^2-OH (1–3 ppm) and – 0.15 ppm μ^1-OH (C) species, and an increase in the μ^1-OH species around 0.4 ppm still occur but to a much more limited extent than those observed for Ag/Al_2O_3-H_2O samples with lower Ag loadings (Fig. 1, spectra c and d). Interestingly, disappearance of the ^{1}H signal at about – 0.10 ppm on the addition of increasing quantities of Ag appears to be completed for Ag(3)/Al_2O_3-H_2O, as detailed in Figure S6 that shows a zoom from – 1 to + 1 ppm of the ^{1}H spectra shown in Fig. 1. Finally, it must be highlighted that the amount of protons was found to remain essentially constant on the addition of increasing quantities of Ag on Al_2O_3-H_2O (Fig. 1, spectra b-f).

Figure S7 shows that exposure of Al_2O_3-H_2O, calcined at 500 °C for 2 h, to NO_x species at RT for 4 h results in a shift of the protons' signals to higher chemical shifts and the vanishing of the μ^1-OH signal at about – 0.10 ppm suggesting the preferential chemisorption of NO_x species in close proximity with such OH groups. A similar trend is observed for Ag (1)/Al_2O_3-H_2O for which not only the signal at about – 0.10 ppm vanishes but also that at about 0.4 ppm, resulting from the introduction of Ag (Fig. 1, spectra b and c), decreases to a significant extent with the exposure of this sample to NO_x (Figure S7**)**.

Information about the environment of the Al atoms close to the hydroxyl groups can be deduced from the ^{1}H–^{27}Al D-HMQC MAS NMR spectrum (Fig. 4). Such an experiment is based on heteronuclear dipolar interaction across space and therefore does not indicate direct bonding of Al atoms to hydroxyl groups, which makes interpretation more delicate as underlined by Völker et al. [82]. Fig. 4 shows that the μ^1-OH groups (A, C and F) at about – 0.1 ppm correlate with aluminum atoms with a very broad signal covering the chemical shifts of tetra- (Al^{IV}, ~ 60 ppm), penta- (Al^{V}, ~ 30 ppm) and hexa-coordinated (Al^{VI}, ~ 10 ppm) aluminum atoms. As already observed in earlier studies [80, 82], this signal is composed of two contributions, the first corresponding to Al^{IV} with a large quadrupolar coupling constant (very broad line with low intensity at 60–20 ppm in the dashed blue rectangle), which are bonded to all types of μ^1-OH hydroxyl groups ((Al^{IV})-μ^1-OH species). The second contribution is due to Al^{VI} species (~7 ppm) not directly bonded to μ^1-OH hydroxyl groups but in their proximity. μ^2-OH groups are bonded to two aluminum atoms and the four types of μ^2-OH groups (B, D, E and G) are found to correlate with Al species exhibiting chemical shifts around 7 ppm. This suggests that, for all μ^2-OH groups, one of these two Al atoms corresponds to Al^{VI} species. For the second Al atoms, the μ^2-OH groups (E), higher in chemical shift (1.55 ppm), could be bonded to Al^{V} species at about 30 ppm, while the other μ^2-OH groups (D, G and B) appear closer to Al^{IV} species. From these observations, the following aluminum atom environments can be proposed for the μ^2-OH species: (Al^{VI} Al^{IV})-μ^2-OH (B), (Al^{VI} Al^{IV})-μ^2-OH (D), (Al^{VI} Al^{V})-μ^2-OH (E), (Al^{VI} Al^{IV})-μ^2-OH (G). The ^{1}H–^{27}Al heteronuclear correlation experiment for Ag(1)/Al_2O_3-H_2O (Figure S8) mainly shows changes in the environment of aluminum atoms bonded to μ^1-OH species. For Ag (1)/Al_2O_3-H_2O, the contribution of Al^{IV} species correlating with μ^1-OH species (A' and F') (Figures S8 and S9), appears to be more intense and narrower than that of Al_2O_3-H_2O (Fig. 4). This suggests a decrease in quadrupolar interaction and thus a more charge-symmetric environment of the Al atoms, probably due to the presence of the silver atoms in close proximity. For Ag(x)/Al_2O_3-H_2O samples containing 2, 3 and 5 wt % of silver (Figures S9-S12), the contribution of Al^{IV} species bonded to μ^1-OH increases steadily, while the contribution of Al^{VI} species near μ^1-OH species remains essentially constant (Figure S9a). The spectra of the Ag/Al_2O_3-H_2O samples containing 2–5 wt% Ag (Figure S9a) show the presence of a new signal at about 70 ppm. The environment of aluminum atoms, close to μ^2-OH species, does not seem to change much with the addition of Ag, which contributes to a decrease in the overall intensity of the signals related to Al^{IV}, Al^{V} and Al^{VI} species due to the decrease in the number of μ^2-OH sites as the amount of silver increases (Figures S9b, S10-12).

It must be highlighted that changes in ^{1}H (Figure S13) and ^{1}H–^{27}Al D-HMQC MAS NMR spectra (Figures S14 and S15) on the addition of Ag on Al_2O_3 appear to be similar to those described in the previous sections for the addition of Ag on the warm-water-pretreated Al_2O_3 support (Al_2O_3-H_2O). Yet one may notice that the vanishing of the μ^1-OH species at about – 0.10 ppm occurs at a lower Ag loading on Al_2O_3 (2 wt%, Figure S13) than on Al_2O_3-H_2O (3 wt%, Fig. 1 and Figure S6).

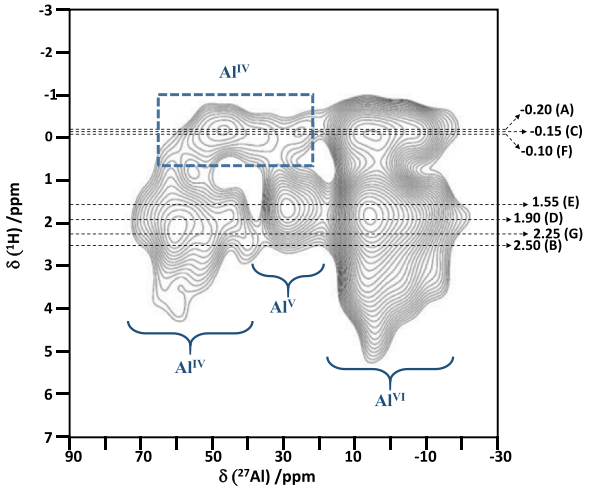

Fig. 4. ^{1}H–^{27}Al D-HMQC MAS NMR spectrum of Al_2O_3-H_2O.

3.3. *Adsorption-desorption of NO_x and (H_2-)C_3H_6-SCR catalytic reactions*

As reported in earlier studies [42,43,59,72], the adsorption-desorption of NO_x from Ag/Al_2O_3 materials have shown unique insights into the comprehensive understanding of the HC-SCR processes by providing unprecedented structure-activity correlations in this field. The characterization of the Ag(x)/Al_2O_3-H_2O series and Ag (4)/Al_2O_3, the latter material acting as a reference sample of the Ag (x)/Al_2O_3 series, by NO_x-TPD is compared to the data acquired previously on Ag(x)/Al_2O_3 [42,43]. In agreement with the profiles already described in our previous studies [42,53], the Ag(x)/Al_2O_3-H_2O series and Ag(4)/Al_2O_3 showed a two-peak desorption profile with a first desorption peak at about 115–200 °C, made of NO mainly and NO_2, and a second peak at about 440 °C essentially due to the release of NO_2, with small amounts of NO (Figure S16a-c) likely due the thermodynamically favored backward reaction of the 2 NO + O_2 = 2 NO_2 equilibrium at the highest temperatures [54]. The introduction of Ag onto Al_2O_3-H_2O led to progressive shift of the temperature of maximum release of NO_x of the low-temperature desorption peak to higher temperatures and a decrease in the intensity of both peaks as the content of Ag increases (Figure S16b), as also observed on the Ag(x)/Al_2O_3 series [42]. The NO_x uptake of Ag(4)/Al_2O_3 (○ in Fig. 5a) estimated from Figure S16c was found to be in good agreement with that expected from the earlier measurements on an Ag(x)/Al_2O_3 series (● in Fig. 5a) [42], thus attesting for the good reproducibility of the synthesis procedure and the reliability of the analytical set-up, as also illustrated in ref. [43]. The NO_x uptakes of the Ag(x)/Al_2O_3-H_2O series appeared to be estimated with a good reproducibility (■ and □ data in Fig. 5a) and were found to be significantly greater than those of the Ag(x)/Al_2O_3 series (● data in Fig. 5a) by about 15–25%. As observed for the Ag(x)/Al_2O_3 series (● data in Fig. 5a), the NO_x uptakes of Ag(x)/Al_2O_3-H_2O series (■ data in Fig. 5a) decreased linearly as the Ag loading increased before levelling off. Whereas the levelling off in the NO_x uptake occurred at an Ag loading close to 2 wt% for the Ag(x)/Al_2O_3 series (● data in Fig. 5a)

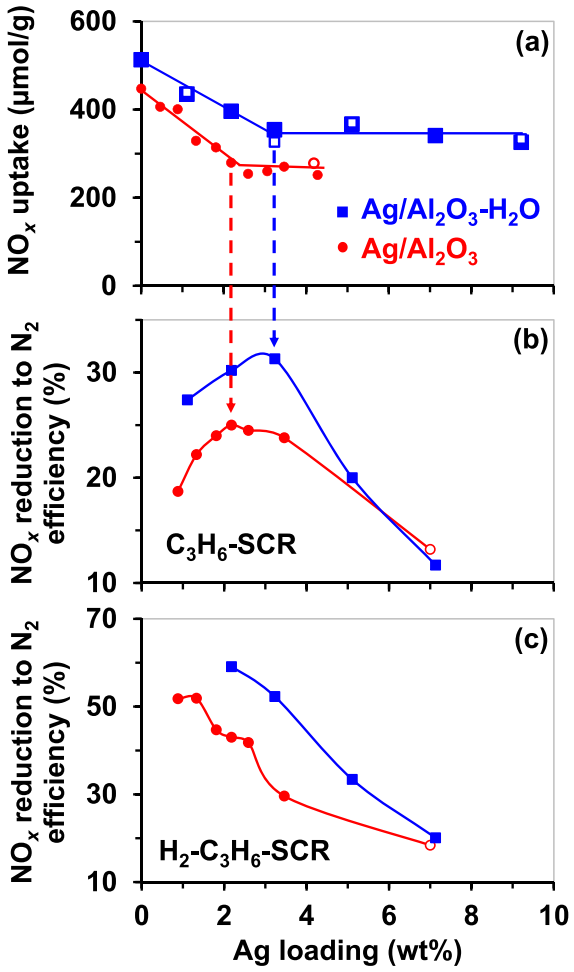

Fig. 5. (a) NO_x uptakes (data from ref. [42] on Ag(x)/Al_2O_3 (●) and recorded on Ag(4)/Al_2O_3 newly synthesized in the present work (○) and on Ag(x)/Al_2O_3-H_2O (■) with duplicate measurements (□)), (b) C_3H_6-SCR (data from ref. [42] on Ag(x)/Al_2O_3 (●) and recorded on Ag(7)/Al_2O_3 (○) and on Ag(x)/Al_2O_3-H_2O (■) newly synthesized in the present work) and (c) H_2-C_3H_6-SCR (data from ref. [42] on Ag(x)/Al_2O_3 (●) and recorded on Ag (x)/Al_2O_3-H_2O (■)) as a function of the Ag loading with an amount of Ag in the catalyst bed that was kept essentially constant to 30.9 ± 1.2 µmol for Ag (x)/Al_2O_3 in ref. [42] and 30.9 ± 0.1 µmol for Ag(x)/Al_2O_3-H_2O. Feed composition: 0 or 0.21% H_2, 385 ppm NO_x, 400 ppm C_3H_6, 8% O_2 and He balance with a 230 mL_{NTP}/min flow rate.

[42], such a levelling off was found to occur at about 3 wt% for the newly synthesized Ag(x)/Al_2O_3-H_2O series (■ data in Fig. 5a). The decrease in NO_x uptake with increasing loadings of Ag up to 2 and 3 wt% for Ag(x)/Al_2O_3 and Ag(x)/Al_2O_3-H_2O, respectively, (Fig. 5a) is assigned to a competition of the Ag and NO_x species for the same alumina surface sites. The levelling off of the NO_x uptake for greater Ag loadings in both series indicates that the number of alumina surface sites for Ag anchoring must be limited on Al_2O_3 and Al_2O_3-H_2O albeit being different in these series. As reported earlier for an Ag loading of about 2 wt% [42] for the Ag(x)/Al_2O_3 series, the NO_x uptake stabilization for Ag loadings greater than or equal to 3 wt% on the newly prepared Ag (x)/Al_2O_3-H_2O series (Fig. 5a) is attributed to the maximum Ag loading for which this metal remains in a highly dispersed state on the freshly calcined Ag(x)/Al_2O_3-H_2O samples, due to the limited number of Ag anchoring sites of the Al_2O_3-H_2O support. At higher Ag loadings than 3 wt%, the additional Ag atoms no longer bind to the Al_2O_3-H_2O surface sites also able to chemisorb NO_x species, explaining that the NO_x uptake remains essentially constant above 3 wt% Ag on Al_2O_3-H_2O (Fig. 5a), and very likely contribute to a growth of the Ag clusters [43].

C_3H_6-SCR and H_2-C_3H_6-SCR catalytic data recorded on the Ag(x)/Al_2O_3-H_2O series and on Ag(7)/Al_2O_3 are shown in Fig. 6. The addition of increasing amount of silver for the Ag(x)/Al_2O_3-H_2O series leads to an increase in the conversion of NO_x to N_2 in C_3H_6-SCR up to an Ag loading of about 3 w%, instead of about 2 wt% in most earlier studies [16,30, 36–38,42], before decreasing at higher Ag loadings. Such a trend is much better illustrated in Fig. 5b, which shows the NO_x reduction efficiency to N_2 of the various Ag(x)/Al_2O_3-H_2O samples, in other words the integration of the NO_x to N_2 trace from 150 to 550 °C normalized to 100% conversion of NO_x to N_2 over the same temperature range as exemplified by the dotted square region in Fig. 6g for C_3H_6-SCR on Ag (3)/Al_2O_3-H_2O. Fig. 5b also shows that pretreatment of Al_2O_3 in warm water prior to Ag deposition leads to catalysts of higher C_3H_6-SCR efficiency compared to those prepared with a non-treated alumina support for Ag loadings lower than 5 wt%. The addition of minute amounts of H_2 in C_3H_6-SCR was found to promote drastically C_3H_6-SCR with a shift to much lower temperatures of the reduction of NO_x to N_2 by about 125–175 °C compared to C_3H_6-SCR from Ag(1)/Al_2O_3-H_2O (Fig. 6a) to Ag(3)/Al_2O_3-H_2O (Fig. 6c), respectively, in agreement with the pioneering finding of Satokawa [17] for H_2-C_3H_8-SCR and the work of Zhang et al. [90] for H_2-C_3H_6-SCR. Whereas the H_2 promoting effect is still observable at the highest silver loadings (Fig. 6e,f), it remains much less pronounced compared to that observed at the lower Ag loadings and therefore less easily quantifiable on a temperature shift basis. Fig. 5c shows that the NO_x to N_2 reduction efficiency improved to a significant extent for the series of samples for which the alumina support had been treated in warm water prior to Ag deposition (■ Ag(x)/Al_2O_3-H_2O) compared to the series of samples prepared on non-pretreated alumina (● Ag(x)/Al_2O_3) for Ag loadings lower than 7 wt%. As reported for Ag (x)/Al_2O_3 samples [43], and in contrast with earlier reports in this field [21,28], the Ag(x)/Al_2O_3-H_2O newly prepared series did not show any optimum Ag content and H_2-C_3H_6-SCR decreased as the Ag loading increased (Fig. 5c). Under the present experimental conditions, Ag (1)/Al_2O_3 appeared to be extremely active for NO_x reduction and reached 100% from 375 to 450 °C so that its efficiency in NO_x reduction to N_2 could not be ascertained reliably and reported in Fig. 5c. The catalytic performance of Ag(2)/Al_2O_3 [42,43] and Ag(2)/Al_2O_3-H_2O, which display similar Ag loadings close to 2.2 wt%, is compared for C_3H_6-SCR (Figure S17a) and H_2-C_3H_6-SCR (Figure S17b). This figure shows that the pretreatment of Al_2O_3 in warm water prior to Ag deposition has little influence on C_3H_6 conversion in C_3H_6-SCR (Figure S17a), while such a pretreatment promotes C_3H_6 conversion in H_2-C_3H_6-SCR at temperatures higher than 250 °C (Figure S17b). It can also be seen from this figure that the better NO_x to N_2 conversion of Ag(2)/Al_2O_3-H_2O occurs at temperatures higher than 400 and 225 °C in C_3H_6-SCR (Figure S17a) and H_2-C_3H_6-SCR (Figure S17b), respectively.

4. Discussion

4.1. Exceeding the 2 wt% Ag optimum loading on Al_2O_3 by pretreating this oxide support in warm water prior to Ag deposition: towards structure-activity correlations

FTIR (Figure S4) and ^{1}H NMR (Fig. 1) clearly indicated that the pretreatment of alumina in warm water increased the OH content of Al_2O_3. Whereas FTIR estimates the increase in OH by about 10% after pretreatment of Al_2O_3 in warm water, this increase appears to be much higher by ^{1}H NMR (about 60%). This discrepancy may be attributed to (i) the fact that the extinction coefficients of the various OH species may be different, while the NMR proton response is known to be independent of the nature of the OH groups, and/or (ii) that the pretreatment of the samples used for both characterization techniques, *i.e.* evacuation at 400 °C in FTIR compared to calcination at 500 °C for ^{1}H NMR (experimental

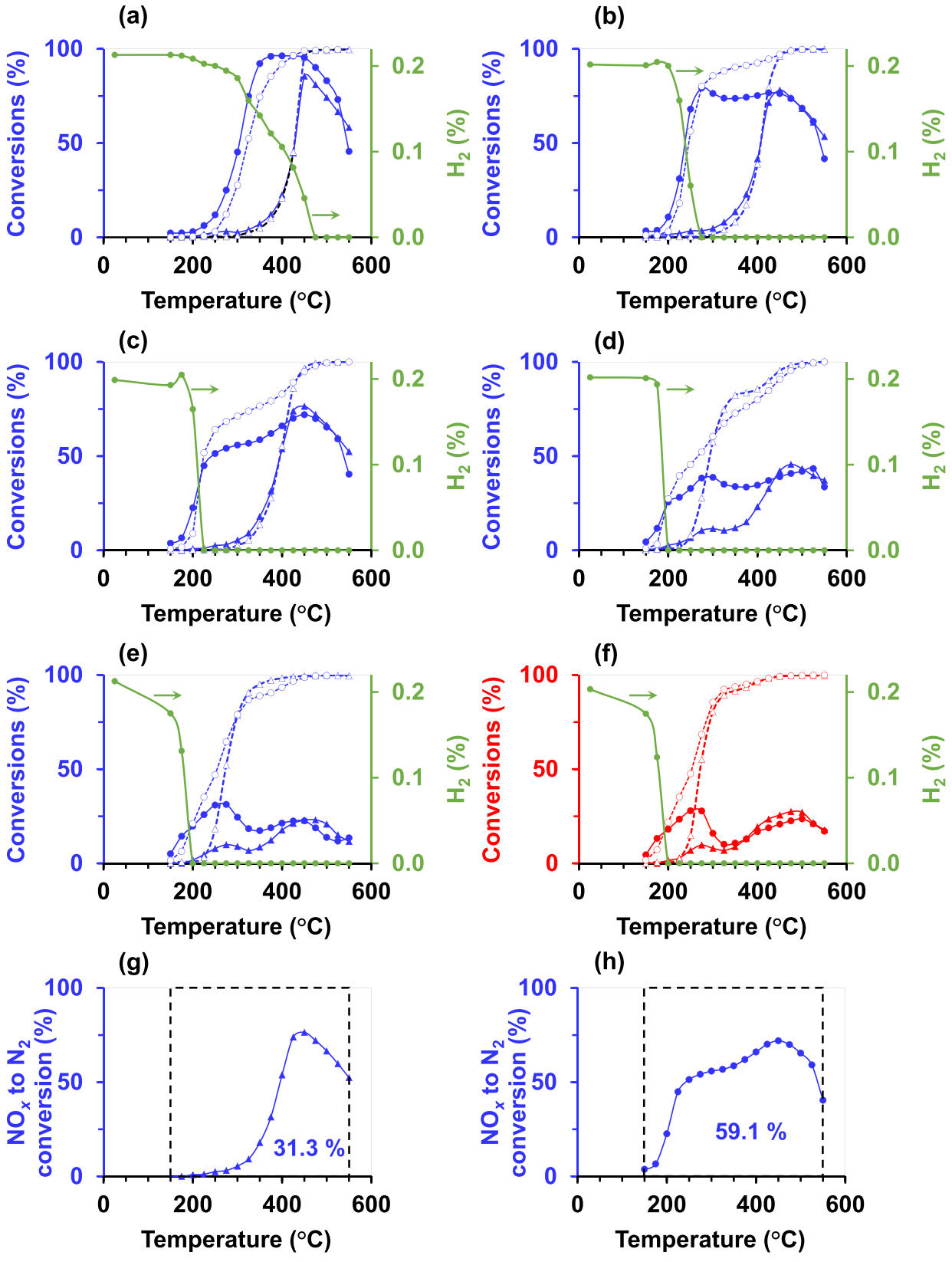

Fig. 6. Influence of the addition of 0.21% H_2 on the conversions of NO_x to N_2 (full symbols) and C_3H_6 to CO_x (open symbols) (C_3H_6-SCR (▲, △) and H_2-C_3H_6-SCR (●, ○) reactions) on (a) Ag(1)/Al_2O_3-H_2O, (b) Ag(2)/Al_2O_3-H_2O, (c) Ag(3)/Al_2O_3-H_2O, (d) Ag(5)/Al_2O_3-H_2O, (e) Ag(7)/Al_2O_3-H_2O and (f) Ag(7)/Al_2O_3 for mechanical mixtures of Ag(x)/Al_2O_3(-H_2O) catalysts and Al_2O_3 for which the amount of Ag was kept essentially constant to 30.9 ± 0.1 μmol. Illustration of the NO_x to N_2 efficiency criterion for C_3H_6-SCR (g) and H_2-C_3H_6-SCR (h) on Ag(3)/Al_2O_3-H_2O. Feed compositions: 0 or 0.21% H_2, 385 ppm NO_x, 400 ppm C_3H_6, 8% O_2 and He balance with a 230 mL_{NTP}/min flowrate. The concentration of H_2 in the course of the H_2-C_3H_6-SCR reaction is also shown (_●_).

section), would lead to more dehydroxylated Al_2O_3 surfaces in the samples investigated by FTIR compared to those investigated by ^1H NMR. As the pretreatment used prior to recording ^1H NMR spectra appeared to be closer to that used of the samples prior to Ag deposition, it can be concluded that the pretreatment of Al_2O_3 in warm water followed by a calcination at 600 °C led to an increase in the OH groups of about 60% in Al_2O_3-H_2O compared to Al_2O_3. It is to be noted that such an increase in the amount of OH groups in Al_2O_3-H_2O cannot be correlated straightforwardly to an increase in its surface area, as the surface area of Al_2O_3-H_2O (~ 195 m^2/g) was found to increase by about 8% only compared to that of Al_2O_3 (~ 180 m^2/g, Table 1). It must also be mentioned that the envelope of the ^1H NMR spectrum of Al_2O_3-H_2O closely resembled that of Al_2O_3 (Fig. 1), which indicates that all types of OH species were increased evenly by the pretreatment of Al_2O_3 in warm water. The changes in Al_2O_3-H_2O may be reasonably attributed to the chemical weathering of alumina [84] and the associated extraction of Al^{3+} cations followed by their precipitation as aluminum hydroxides and their transformation to transition aluminas, hardly differentiable by XRD, after a calcination step (Figure S2). The occurrence of dissolution-precipitation phenomena during the pretreatment of Al_2O_3 in warm water is supported by the changes in surface morphology of the Al_2O_3 grains observed by SEM. Figure S3 indeed shows the appearance of micrometric bayerite and Al_2O_3 platelets on the surface of the Al_2O_3 grains after pretreatment of the pristine support in warm water and further calcination, respectively.

More interestingly, it was found that the pretreatment of Al_2O_3 in warm water prior to Ag deposition led to significantly more active silver alumina catalysts (Fig. 5b,c, ■ Ag(x)/Al_2O_3-H_2O) compared to those prepared with the pristine Al_2O_3 support (Fig. 5b,c, ● Ag(x)/Al_2O_3) for Ag loadings lower than 5 and 7 wt% for C_3H_6-SCR (Fig. 5b) and H_2-C_3H_6-SCR (Fig. 5c), respectively. In addition, the optimum loading of Ag for C_3H_6-SCR (Fig. 5b, ● Ag(x)/Al_2O_3), and widely accepted in the field as 2 wt% on Al_2O_3 [16,30,36–38,42], was found to be shifted to about 3 wt% for the catalysts prepared from the Al_2O_3 support pretreated in warm water prior to Ag deposition (Fig. 5b, ■ Ag(x)/Al_2O_3-H_2O). To our knowledge, such a shift in the optimum Ag loading in C_3H_6-SCR due to the pretreatment of Al_2O_3 has never been reported to date. This shift in optimum Ag loading for C_3H_6-SCR can be remarkably correlated to the characterization of the Al_2O_3 support of the Ag(x)/Al_2O_3-H_2O samples by NO_x-TPD (Fig. 5a,b, ■ Ag(x)/Al_2O_3-H_2O, blue dotted arrow) for which optimum C_3H_6-SCR catalytic activity is found to perfectly match the Ag loading at which the NO_x uptake starts to remain essentially constant, as also reported earlier [42] in the case of a Ag(x)/Al_2O_3 (Fig. 5a,b, ● Ag(x)/Al_2O_3, red dotted arrow). Such a unique NO_x-TPD–C_3H_6-SCR structure–activity correlation provides further support on the usefulness of the characterization of the Al_2O_3 supporting oxide of Ag/Al_2O_3 catalysts by NO_x-TPD and can be used as a reliable descriptor of the efficiency of the silver alumina catalysts in the field of C_3H_6-SCR. One may argue that our preliminary work on the influence of the pretreatment of Al_2O_3 in warm water prior to Ag deposition would refute such a statement, as in this previous work an improvement in H_2-C_3H_6-SCR performance only was observed on Ag(1.8)/Al_2O_3-OH [72]. Despite the difference in the duration of the pretreatment Al_2O_3 in warm water, it must be highlighted that Ag was deposited on a dried pretreated sample in this earlier work [72], whereas the samples studied in the present work were prepared on a warm-water-treated support that was subsequently dried and calcined prior to Ag deposition. Hence this difference in pretreatment prior to Ag deposition may be at the origin of such apparently conflicting results. It is also important to note that the shift in optimum Ag loading from about 2 (Ag(x)/Al_2O_3) to about 3 wt% (Ag(x)/Al_2O_3-H_2O), *i.e.* about 50% increase, in C_3H_6-SCR performance (Fig. 5b) and NO_x uptake stabilization (Fig. 5a) remarkably agrees with the increase in OH species quantified by ^1H NMR (Fig. 1), *i.e.* about 60%. In addition, the present NMR data unprecedentedly show that Ag (Fig. 1 and Figure S13) and NO_x (Figure S7) perturbs the same μ^1-OH species of Al_2O_3, pretreated or not in warm water, which is fully consistent with the decrease in NO_x uptake observed as the loading of Ag increases at low Ag loadings in both silver alumina series (Fig. 5a). Identification of the adsorption sites of NO_x on Al_2O_3 remains challenging. In addition to the potential interaction of NO_x species with Al^{3+} and O^{2-} surface sites [91–93], earlier FTIR studies have highlighted on the disappearance of part of the OH groups of Al_2O_3 after exposure to various NO_x atmospheres [91,93]. Szanyi et al. also concluded that most of the consumed OH groups were not restored during TPD following the NO_2 uptake experiments [93]. These observations are consistent with the OH-assisted formation of nitrates ($3\ NO_2 + 2\ OH^- = 2\ NO_3^- + NO + H_2O$) proposed earlier by Hadjiivanov and co-workers over TiO_2 [94]. Considering all of the above, the greater NO_x uptake of Al_2O_3-H_2O compared to Al_2O_3 (Fig. 5a) can be reasonably attributed, at least partly, to an increase in the OH content of Al_2O_3-H_2O compared to Al_2O_3 (Fig. 1). Finally, a remarkable correlation can also be established between the vanishing of the μ^1-OH species at about – 0.10 ppm that occurred at about 2 and 3 wt% Ag for ^1H NMR spectra of the Ag (x)/Al_2O_3 (Figure S13) and Ag(x)/Al_2O_3-H_2O (Fig. 1) series, respectively, and the corresponding NO_x uptakes (Fig. 5a) and C_3H_6-SCR performance (Fig. 5b). All of the above could indicate that a key parameter in the synthesis of silver alumina catalyst to preserve Ag in a highly dispersed state [42] would lie in the amount of OH species available on the Al_2O_3 supporting oxide. Such a conclusion would be consistent with the earlier statement of Zhang and Kaliaguine [60] and Wang et al. [63] on the potential exchange process between Ag^+ ions and some protons of Al_2O_3 during the conventional impregnation step to lead to Ag-O-Al species. This justifies the works done by several groups on the use of various Al_2O_3 precursors [60,61], on the morphology of Al_2O_3 [62–64] and on ball-milled Al_2O_3 supports [69,71] to improve HC-SCR performance. This OH key parameter could also help reconcile earlier literature data for which optimum Ag loading was unexpectedly determined to be 4 wt% [95], rather than the commonly accepted loading of 2 wt% [16,30,36–38,42], for which the used Al_2O_3 may have exhibited a much greater proportion of OH groups of interest as anchoring sites of Ag.

The present series of Ag(x)/Al_2O_3-H_2O was therefore subjected to in-depth NMR investigations to help unravel the Al_2O_3 sites of importance in the anchoring of Ag.

4.2. *Unravelling of the alumina sites of importance for anchoring Ag: a NMR-assisted study*

As indicated in the NMR result section, the ^1H–^1H DQSQ MAS spectrum of Al_2O_3-H_2O (Fig. 3a) was found to be identical to that reported by Merle et al. [80] and therefore used for the assignation of the protons of the present study. While various combinations of protons have been proposed in the work Merle et al. [80], their preferential location on the Al_2O_3 crystallites has not been attempted. By combining NMR measurements and DFT modelling, based on revisited models for the (100), (111), basal $(110)_b$ and lateral $(110)_l$ facets of γ-Al_2O_3, Batista et al. recently provided further insights into the location of the various protons on the Al_2O_3 crystallites [81]. In their study, Batista et al. showed the proximity of μ^1-OH species (located on the edge defined by the intercept of the basal $(110)_b$ and (100) facets, and noted as $(110)_b$/(100) edge) and μ^2-OH species (located on the basal $(110)_b$ facet near the $(110)_b$/(100) edge), which are themselves close to μ^2-OH species (located on basal $(110)_b$ facets) [81]. Given that the NMR fingerprints of the OH species identified in the present work are fairly consistent with those reported earlier by Merle et al. [80] for a comparable alumina carrier, and that Batista et al. investigated the surface location of the OH species on model alumina crystallites [81], we tentatively assigned the location of the various (A-G) hydroxyl groups (Fig. 7). We propose that μ^1-OH $(110)_b$/(100) edge, μ^2-OH on the basal $(110)_b$ facet near the $(110)_b$/(100) edge and μ^2-OH $(110)_b$ facets species could be attributed to μ^1-OH (C), μ^2-OH (D) and μ^2-OH (E) species,

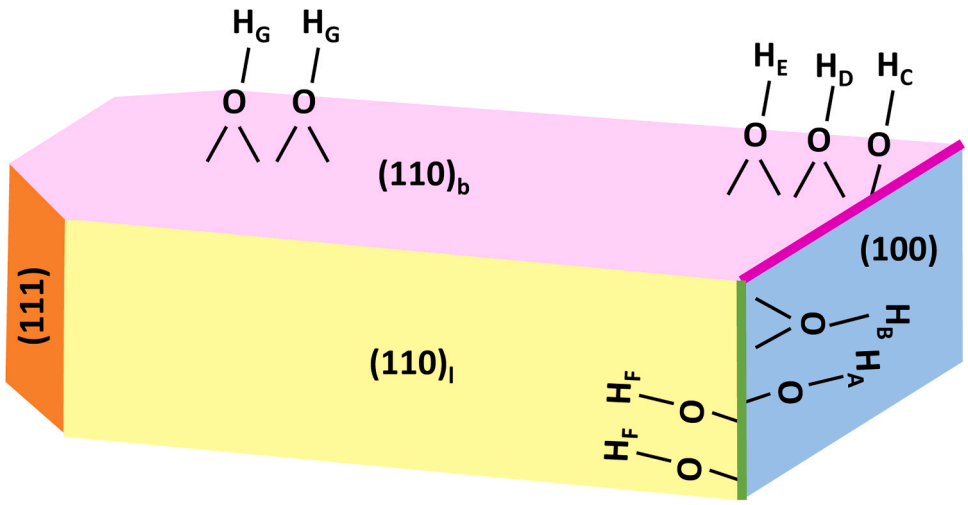

Fig. 7. Proposed location of the A-G hydroxyl species on the model Al_2O_3 crystallite reported by Batista et al. [81].

respectively. In addition, Batista et al. predicted the presence of two μ^1-OH species located on the (100)/(110)$_l$ edge. The first ones are in close proximity with identical μ^1-OH species and could be attributed to μ^1-OH (F) species. The second ones are close to μ^2-OH species located on the (100) facet near the (100)/(110)$_l$ edge [81] and could be assigned to μ^1-OH (A) and μ^2-OH (B), respectively. Finally, μ^2-OH species on basal (110)$_b$ and lateral (110)$_l$ facets of γ-Al_2O_3 close to each other could be assigned to μ^2-OH (G) species.

As already stated in the preceding section, Ag anchoring has been proposed to occur on the alumina surface via substitution of a proton from an OH group and eventually leading to the formation of Al-O-Ag species [60,63,75]. From the comparison of the NMR data of Al_2O_3-H_2O and Ag(1)/Al_2O_3-H_2O (Fig. 1, Fig. 3a, Fig. 3b), the increase in the signal of the μ^1-OH species at about 0.4 ppm, and the decrease in those of μ^1-OH at about – 0.10 ppm and μ^2-OH at about 2.5 ppm may be accounted for by the grafting of Ag on a μ^1-OH group, issued from the rehydroxylation of the μ^2-OH species during the Ag impregnation step of Al_2O_3-H_2O, and located near the (100)/(110)$_l$ edge (Fig. 8c). Such a grafting leads to the shift of μ^1-OH (A) at – 0.2 ppm and (F) at – 0.1 ppm of Al_2O_3-H_2O (Fig. 8a) to μ^1-OH (A') and (F') at about 0.4 ppm due to Ag perturbation on Ag(1)/Al_2O_3-H_2O (Fig. 8c), and the creation of new μ^1-OH (N) species on the (100) facets at the expense of those of μ^2-OH (B) at 2.5 ppm. The chemical shift of this newly formed μ^1-OH (N) species on Ag(1)/Al_2O_3-H_2O should also be of about 0.4 ppm, as the intensity of this signal increases to a much greater extent than the decrease in the μ^1-OH (A) and (F), and μ^2-OH (B) signals (Fig. 1). Such an Ag grafting would also account for the increase and the narrowing of the signal corresponding to (Al^{IV})-μ^1-OH species (Figure S9), whereas the interference caused by the presence of silver disturb the environment of Al^{VI} species, leading to a narrowing of the signal at about 7 ppm in the ^{27}Al dimension of D-HMQC experiment (Figure S9). For Ag (2)/Al_2O_3-H_2O, similar Ag grafting should also applies and the essentially constant μ^2-OH (B) may be attributed to an overlapping of this signal with the signal at 0.4 ppm, which increases drastically when the Ag loading increases from about 1 to about 2 wt%. The fact, on the one hand, that the signal at 0.4 ppm remains essentially constant and that the signal at – 0.15 ppm disappears at Ag loadings greater than 2 wt% and on the other hand, that the signal at about 2 ppm decreases at Ag loadings greater than or equal to 3 wt% (Fig. 1, spectra e,f) suggests an additional anchoring of Ag onto μ^2-OH (D) species located on the (110)$_b$

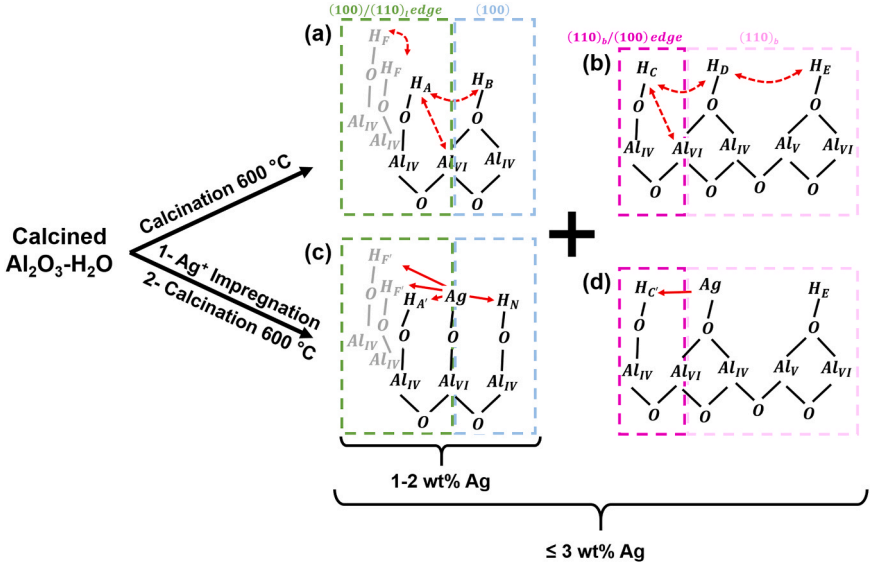

Fig. 8. Description of the various proton environments on γ-Al_2O_3 and schematic representation of the influence of the addition of Ag on the OH groups of γ-Al_2O_3. The dotted double arrows show nuclei that could be probed by ^{1}H–^{1}H DQSQ MAS and ^{1}H–^{27}Al D-HMQC MAS NMR, while simple arrows show how silver influences the signals of the neighboring protons. The colors of the dotted boxes correspond to those used for the edges and planes of the Al_2O_3 crystallite shown in Fig. 7.

facets and close the $(110)_b/(100)$ edge (Fig. 8d) and a shift of the μ^1-OH (C) species at – 0.15 ppm to 0.4 ppm (μ^1-OH (C')). The presence of Ag atoms in the proximity of (Al^{IV})-μ^1-OH (A', C', F' and N) species may account for by the appearance of the new Al^{IV} signal at about 70 ppm (Figure S9).

In summary, the present in depth NMR study allowed us to conclude to the grafting of Ag (i) preferentially on μ^1-OH groups of Al_2O_3-H_2O, in agreement with the earlier studies [63,75], up to a loading of about 3 wt % Ag that would be located near the $(100)/(110)_l$ edge and then near the $(110)_b/(100)$ edge of Al_2O_3 crystallites and (ii) on μ^2-OH groups of Al_2O_3-H_2O at higher Ag loadings (Fig. 8).

The FTIR band at 3730 cm^{-1} has been commonly assigned in earlier literature reports to the vibration of μ^2-OH groups [63,80], and references therein. The observed increase in intensity of this band on the addition of Ag on Al_2O_3-H_2O (Figure S4b), together with the fact that the ^1H signal at 0.4 ppm, -unambiguously assigned to μ^1-OH species-, was found to be the only one to increase in ^1H spectra (Fig. 1) therefore question the original FTIR assignation of the band at 3730 cm^{-1} as μ^2-OH vibrators.

The finite number of μ^1-OH Ag anchoring species on the edges of Al_2O_3 may therefore be at the origin of the limited amount of Ag able to be accommodated on Al_2O_3 in a highly dispersed state to form the catalytic Ag species and/or to act their precursor in the (H_2)-C_3H_6-SCR reactions. This finite number of μ^1-OH Ag anchoring species on the edges of Al_2O_3 would be at the origin of the well-known existence of an optimum loading of Ag on Al_2O_3 for C_3H_6-SCR [42]. Li et al. recently took advantage of such a peculiarity to lower the amount of Ag introduced on Al_2O_3 by poisoning its Ag anchoring sites by copper prior to introduction of Ag [96]. This original approach was reported to provide Ag-low-loaded Ag-CuO_x/Al_2O_3 catalysts with enhanced activity and selectivity for the catalytic oxidation of ammonia compared to their Ag/Al_2O_3 counterparts.

5. Conclusion

The present work shows that pretreatment of pristine Al_2O_3 in warm water prior to Ag deposition allows to prepare catalysts of significantly higher performance in (H_2-)C_3H_6-SCR compared to conventional Ag/Al_2O_3 catalysts. In addition, remarkable NO_x-TPD-C_3H_6-SCR structure-activity correlations indicate that optimum composition of the Ag/Al_2O_3 catalysts can be improved by about 50% in terms of Ag content for the first time, leading to an optimum composition of about 3 wt% Ag on Al_2O_3-H_2O compared to about 2 wt% on pristine Al_2O_3. Combining ^1H–^1H DQSQ MAS and ^1H–^{27}Al D-HMQC MAS NMR in-depth unprecedented NMR investigations on Ag-Al_2O_3 samples and a thorough literature survey of most recent investigations performed on Al_2O_3 in this field, allowed us to identify the alumina sites of importance in the anchoring of Ag. These sites are proposed to be μ^1-OH groups located near the $(100)/(110)_l$ edge and then near the $(110)_b/(100)$ edge of Al_2O_3 crystallites and bonded to octahedrally coordinated Al species. This study, the first of its kind, paves the way to further improvements in the comprehensive understanding of Al_2O_3 and in particular the deposition of Ag on Al_2O_3, which may be broaden to the deposition of other transition metals on such a widely used supporting oxide.

CRediT authorship contribution statement

Yannick Millot: Writing – review & editing, Writing – original draft, Visualization, Investigation, Data curation, Conceptualization. **Guylène Costentin:** Writing – review & editing. **Clémence Rodigue:** Investigation, Data curation. **Thomas Onfroy:** Writing – review & editing, Investigation, Data curation. **Cyril Thomas:** Writing – review & editing, Writing – original draft, Visualization, Validation, Supervision, Resources, Project administration, Investigation, Data curation, Conceptualization.

Declaration of Competing Interest

The authors declare that they have no known competing financial interests or personal relationships that could have appeared to influence the work reported in this paper.

Data Availability

Data will be made available on request.

Acknowledgments

The authors thank Sorbonne Université and CNRS for providing funding (Crédits récurrents) and access to the analytical equipment used in the present work. The authors also acknowledge S. Koné-Guira, Dr. J. Schnee and S. Casale for recording the N_2 sorption isotherms on about half of the samples listed in Table 1, the XRD patterns of the vacuum-dried and calcined Al_2O_3-H_2O samples (Figure S2), and the SEM images (Figure S3), respectively. The SEM microscope and NMR spectrometer used in the present work belonging to the Fédération de Chimie et Matériaux de Paris-Centre (FCMat, Fédération de Recherche 2482) were funded by UPMC, CNRS and Région Ile de France.

Appendix A. Supporting information

Supplementary data associated with this article can be found in the online version at doi:10.1016/j.apcatb.2024.123975.

References

[1] EEA, Air quality in Europe 2022, (2022) ⟨https://www.eea.europa.eu//publications/air-quality-in-europe-2022⟩.
[2] World's Air Pollution: Real-time Air Quality Index, ⟨https://waqi.info⟩.
[3] DirectivE (EU) 2016/2284 OF the European Parliament and of the Council of 14 December 2016 on the Reduction of National Emissions of Certain Atmospheric Pollutants, Amending Directive 2003/35/EC and repealing Directive 2001/81/EC, Official Journal of the European Union, (2016) L 344/341- L334/331, ⟨http://data.europa.eu/eli/dir/2016/2284/oj⟩.
[4] (2023) ⟨https://www.eea.europa.eu/data-and-maps/indicators/eea-32-sulphur-dioxide-so32-emissions-31/assessment-33⟩.
[5] (2023) ⟨https://www.citepa.org/fr/2020-nox/⟩.
[6] Total emissions of nitrogen oxide (NOx) in the European Union (EU-27) from 1990 to 2021, (2023) ⟨https://www.statista.com/statistics/1171343/nitrogen-oxide-emissions-european-union-eu-1171328/#:~:text=Nitrogen%1171320oxide%1171320⟩(NOx)%1171320emissions%1171320in,by%1172063%1171320percent%1171320since%1201990.
[7] E. Mulholland, J. Miller, Y. Bernard, K. Lee, F. Rodríguez, The role of NO_x emission reductions in Euro 7/VII vehicle emission standards to reduce adverse health impacts in the EU27 through 2050, Transp. Eng. 9 (2022) 100133, https://doi.org/10.1016/j.treng.2022.100133.
[8] K.C. Taylor, Nitric oxide catalysis in automotive exhaust systems, Catal. Rev. Sci. Eng. 35 (1993) 457–481, https://doi.org/10.1080/01614949308013915.
[9] R. Burch, Knowledge and know-how in emission control for mobile applications, Catal. Rev. 46 (2004) 271–334, https://doi.org/10.1081/CR-200036718.
[10] I. Nova, E. Tronconi, Urea-SCR Technology for deNO_x after Treatment of Diesel Exhausts, Springer, 2014, https://doi.org/10.1007/978-1-4899-8071-7.
[11] L. Han, S. Cai, M. Gao, J.-y Hasegawa, P. Wang, J. Zhang, L. Shi, D. Zhang, Selective catalytic reduction of NO_x with NH_3 by using novel catalysts: state of the art and future prospects, Chem. Rev. 119 (2019) 10916–10976, https://doi.org/10.1021/acs.chemrev.9b00202.
[12] W.S. Epling, L.E. Campbell, A. Yezerets, N.W. Currier, J.E. Parks, Overview of the fundamental reactions and degradation mechanisms of NO_x storage/reduction catalysts, Catal. Rev. 46 (2004) 163–245, https://doi.org/10.1081/CR-200031932.
[13] I. Nova, E. Bill, P. Chuck, Challenges for catalytic exhaust aftertreatment, Catal. Today 231 (2014) 1–2, https://doi.org/10.1016/j.cattod.2014.02.017.
[14] K.-i Shimizu, A. Satsuma, Selective catalytic reduction of NO over supported silver catalysts—practical and mechanistic aspects, Phys. Chem. Chem. Phys. 8 (2006) 2677–2695,, https://doi.org/10.1039/B601794K.
[15] R. Burch, J. Breen, F. Meunier, A review of the selective reduction of NO_x with hydrocarbons under lean-burn conditions with non-zeolitic oxide and platinum group metal catalysts, Appl. Catal. B Environ. 39 (2002) 283–303, https://doi.org/10.1016/S0926-3373(02)00118-2.
[16] T. Miyadera, Alumina-supported silver catalysts for the selective reduction of nitric oxide with propene and oxygen-containing organic compounds, Appl. Catal. B Environ. 2 (1993) 199–205, https://doi.org/10.1016/0926-3373(93)80048-I.

[17] S. Satokawa, Enhancing the NO/C_3H_8/O_2 reaction by using H_2 over Ag/Al_2O_3 catalysts under lean-exhaust conditions, Chem. Lett. 29 (2000) 294–295, https://doi.org/10.1246/cl.2000.294.

[18] S. Satokawa, J. Shibata, K.-I. Shimizu, A. Satsuma, T. Hattori, Promotion effect of H_2 on the low temperature activity of the selective reduction of NO by light hydrocarbons over Ag/Al_2O_3, Appl. Catal. B Environ. 42 (2003) 179–186, https://doi.org/10.1016/S0926-3373(02)00231-X.

[19] K.-i Shimizu, A. Satsuma, T. Hattori, Catalytic performance of Ag–Al_2O_3 catalyst for the selective catalytic reduction of NO by higher hydrocarbons, Appl. Catal. B Environ. 25 (2000) 239–247, https://doi.org/10.1016/S0926-3373(99)00135-6.

[20] K.-i Shimizu, J. Shibata, A. Satsuma, T. Hattori, Mechanistic causes of the hydrocarbon effect on the activity of Ag–Al_2O_3 catalyst for the selective reduction of NO, Phys. Chem. Chem. Phys. 3 (2001) 880–884, https://doi.org/10.1039/B007382M.

[21] N. Sadokhina, A. Prokhorova, R. Kvon, I. Mashkovskii, G. Bragina, G. Baeva, V. Bukhtiyarov, A.Y. Stakheev, Dependence of the catalytic activity of Ag/Al_2O_3 on the silver concentration in the selective reduction of NO_x with *n*-hexane in the presence of H_2, Kinet. Catal. 53 (2012) 107–116, https://doi.org/10.1134/S0023158412010090.

[22] P. Sazama, L. Čapek, H. Drobná, Z. Sobalik, J. Dědeček, K. Arve, B. Wichterlová, Enhancement of decane-SCR-NO_x over Ag/alumina by hydrogen. Reaction kinetics and in situ FTIR and UV–vis study, J. Catal. 232 (2005) 302–317, https://doi.org/10.1016/j.jcat.2005.03.013.

[23] S. Kameoka, T. Chafik, Y. Ukisu, T. Miyadera, Role of organic nitro compounds in selective reduction of NO_x with ethanol over different supported silver catalysts, Catal. Lett. 51 (1998) 11–14, https://doi.org/10.1023/A:1019041118880.

[24] S. Chansai, R. Burch, C. Hardacre, D. Norton, X. Bao, L. Lewis, Investigating the promotional effect of methanol on the low temperature SCR reaction on Ag/Al_2O_3, Appl. Catal. B Environ. 160 (2014) 356–364, https://doi.org/10.1016/j.apcatb.2014.05.040.

[25] M. Männikkö, X. Wang, M. Skoglundh, H. Härelind, Silver/alumina for methanol-assisted lean NO_x reduction—On the influence of silver species and hydrogen formation, Appl. Catal. B Environ. 180 (2016) 291–300, https://doi.org/10.1016/j.apcatb.2015.06.002.

[26] N. Popovych, P. Kirienko, S. Soloviev, S. Orlyk, Selective catalytic reduction of NO_x by C_2H_5OH over Ag/Al_2O_3/cordierite: effect of the surface concentration of silver, Catal. Today 191 (2012) 38–41, https://doi.org/10.1016/j.cattod.2012.01.039.

[27] J.A. Pihl, T.J. Toops, G.B. Fisher, B.H. West, Selective catalytic reduction of nitric oxide with ethanol/gasoline blends over a silver/alumina catalyst, Catal. Today 231 (2014) 46–55, https://doi.org/10.1016/j.cattod.2013.12.042.

[28] K.-I. Shimizu, M. Tsuzuki, K. Kato, S. Yokota, K. Okumura, A. Satsuma, Reductive activation of O_2 with H_2-reduced silver clusters as a key step in the H_2-promoted selective catalytic reduction of NO with C_3H_8 over Ag/Al_2O_3, J. Phys. Chem. C 111 (2007) 950–959, https://doi.org/10.1021/jp066147f.

[29] H. Kannisto, M. Skoglundh, K. Arve, E. Olsson, H. Härelind, Direct observation of atomically-resolved silver species on a silver alumina catalyst active for selective catalytic reduction of nitrogen oxides, Catal. Sci. Technol. 9 (2019) 6213–6216, https://doi.org/10.1039/C9CY00940J.

[30] K.-i Shimizu, J. Shibata, H. Yoshida, A. Satsuma, T. Hattori, Silver-alumina catalysts for selective reduction of NO by higher hydrocarbons: structure of active sites and reaction mechanism, Appl. Catal. B Environ. 30 (2001) 151–162, https://doi.org/10.1016/S0926-3373(00)00229-0.

[31] O. Gorce, F. Baudin, C. Thomas, P. Da Costa, G. Djéga-Mariadassou, On the role of organic nitrogen-containing species as intermediates in the hydrocarbon-assisted SCR of NO_x, Appl. Catal. B Environ. 54 (2004) 69–84, https://doi.org/10.1016/j.apcatb.2004.05.022.

[32] S. Chansai, R. Burch, C. Hardacre, J. Breen, F. Meunier, The use of short time-on-stream in situ spectroscopic transient kinetic isotope techniques to investigate the mechanism of hydrocarbon selective catalytic reduction (HC-SCR) of NO_x at low temperatures, J. Catal. 281 (2011) 98–105, https://doi.org/10.1016/j.jcat.2011.04.006.

[33] S. Chansai, R. Burch, C. Hardacre, J. Breen, F. Meunier, Investigating the mechanism of the H_2-assisted selective catalytic reduction (SCR) of NO_x with octane using fast cycling transient in situ DRIFTS-MS analysis, J. Catal. 276 (2010) 49–55, https://doi.org/10.1016/j.jcat.2010.08.014.

[34] P.S. Kim, M.K. Kim, B.K. Cho, I.-S. Nam, S.H. Oh, Effect of H_2 on deNO_x performance of HC-SCR over Ag/Al_2O_3: morphological, chemical, and kinetic changes, J. Catal. 301 (2013) 65–76, https://doi.org/10.1016/j.jcat.2013.01.026.

[35] E.G. Ragoyja, V.E. Matulis, O.A. Ivashkevich, D.A. Lyakhov, D. Michels, DFT study of the NO reduction mechanism on Ag/γ-Al_2O_3 catalysts, J. Phys. Chem. C 127 (2023) 7131–7141, https://doi.org/10.1021/acs.jpcc.2c09042.

[36] T. Hoost, R. Kudla, K. Collins, M. Chattha, Characterization of Ag/γ-Al_2O_3 catalysts and their lean-NO_x properties, Appl. Catal. B Environ. 13 (1997) 59–67, https://doi.org/10.1016/S0926-3373(96)00090-2.

[37] L.-E. Lindfors, K. Eränen, F. Klingstedt, D.Y. Murzin, Silver/alumina catalyst for selective catalytic reduction of NO_x to N_2 by hydrocarbons in diesel powered vehicles, Top. Catal. 28 (2004) 185–189, https://doi.org/10.1023/B:TOCA.0000024349.28158.f3.

[38] K. Arve, L. Čapek, F. Klingstedt, K. Eränen, L.-E. Lindfors, D.Y. Murzin, J. Dědeček, Z. Sobalik, B. Wichterlová, Preparation and characterisation of Ag/alumina catalysts for the removal of NO_x emissions under oxygen rich conditions, Top. Catal. 30 (2004) 91–95, https://doi.org/10.1023/B:TOCA.0000029734.85321.ef.

[39] K. Lee, B. Choi, C. Kim, C. Lee, K. Oh, De-NOx characteristics of HC-SCR system employing combined Ag/Al_2O_3 and CuSn/ZSM-5 catalyst, J. Ind. Eng. Chem. 93 (2021) 461–475, https://doi.org/10.1016/j.jiec.2020.10.026.

[40] H.Y. Law, J. Blanchard, X. Carrier, C. Thomas, NO_x-TPD as a tool to estimate the accessible zirconia surface of ZrO_2-containing materials, J. Phys. Chem. C 114 (2010) 9731–9738,, https://doi.org/10.1021/jp9089535.

[41] C. Thomas, Should W surface density of WO_x−ZrO_2 catalysts be calculated with respect to the specific surface area of the sample or that of ZrO_2 only? J. Phys. Chem. C 115 (2011) 2253–2256,, https://doi.org/10.1021/jp110497e.

[42] T. Chaieb, L. Delannoy, C. Louis, C. Thomas, On the origin of the optimum loading of Ag on Al_2O_3 in the C_3H_6-SCR of NO_x, Appl. Catal. B Environ. 142 (2013) 780–784, https://doi.org/10.1016/j.apcatb.2013.06.010.

[43] T. Chaieb, L. Delannoy, G. Costentin, C. Louis, S. Casale, R.L. Chantry, Z. Li, C. Thomas, Insights into the influence of the Ag loading on Al_2O_3 in the H_2-assisted C_3H_6-SCR of NO_x, Appl. Catal. B Environ. 156 (2014) 192–201, https://doi.org/10.1016/j.apcatb.2014.03.025.

[44] M. Richter, U. Bentrup, R. Eckelt, M. Schneider, M.-M. Pohl, R. Fricke, The effect of hydrogen on the selective catalytic reduction of NO in excess oxygen over Ag/Al_2O_3, Appl. Catal. B Environ. 51 (2004) 261–274, https://doi.org/10.1016/j.apcatb.2004.02.015.

[45] K.-i Shimizu, J. Shibata, A. Satsuma, Kinetic and in situ infrared studies on SCR of NO with propane by silver–alumina catalyst: role of H_2 on O_2 activation and retardation of nitrate poisoning, J. Catal. 239 (2006) 402–409, https://doi.org/10.1016/j.jcat.2006.02.011.

[46] P. Sazama, B. Wichterlová, Selective catalytic reduction of NO_x by hydrocarbons enhanced by hydrogen peroxide over silver/alumina catalysts, Chem. Commun. (2005) 4810–4811,, https://doi.org/10.1039/B507553J.

[47] H. Kannisto, H.H. Ingelsten, M. Skoglundh, Aspects of the role of hydrogen in H_2-assisted HC–SCR Over Ag–Al_2O_3, Top. Catal. 52 (2009) 1817–1820,, https://doi.org/10.1007/s11244-009-9359-1.

[48] S.T. Korhonen, A.M. Beale, M.A. Newton, B.M. Weckhuysen, New insights into the active surface species of silver alumina catalysts in the selective catalytic reduction of NO, J. Phys. Chem. C 115 (2011) 885–896, https://doi.org/10.1021/jp102530y.

[49] R. Burch, J. Breen, C. Hill, B. Krutzsch, B. Konrad, E. Jobson, L. Cider, K. Eränen, F. Klingstedt, L.-E. Lindfors, Exceptional activity for NO_x reduction at low temperatures using combinations of hydrogen and higher hydrocarbons on Ag/Al_2O_3 catalysts, Top. Catal. 30 (2004) 19–25, https://doi.org/10.1023/B:TOCA.0000029722.12588.1f.

[50] J.P. Breen, R. Burch, C. Hardacre, C.J. Hill, Structural investigation of the promotional effect of hydrogen during the selective catalytic reduction of NO_x with hydrocarbons over Ag/Al_2O_3 catalysts, J. Phys. Chem. B 109 (2005) 4805–4807,, https://doi.org/10.1021/jp050253k.

[51] K. Ralphs, C.D. Agostino, R. Burch, S. Chansai, L.F. Gladden, C. Hardacre, S. L. James, J. Mitchell, S.F. Taylor, Assessing the surface modifications following the mechanochemical preparation of a Ag/Al_2O_3 selective catalytic reduction catalyst, Catal. Sci. Technol. 4 (2014) 531–539, https://doi.org/10.1039/C3CY00945A.

[52] N. El Kolli, C. Potvin, C. Thomas, Evidence for the facile formation of nitrogen-containing compounds from NO_x and propene species on tungstated zirconia-based catalysts: Are these compounds active or spectator species in the selective catalytic reduction of NO_x by C_3H_6? J. Catal. 259 (2008) 240–249, https://doi.org/10.1016/j.jcat.2008.08.009.

[53] K. Malinger, J. Blanchard, R.P. Doherty, C. Thomas, Organo-NO_x formation–decomposition as the origin of the changes in the low temperature NO-TPD profile in the presence of *n*-decane on Ag/γ-Al_2O_3, Catal. Commun. 46 (2014) 81–85, https://doi.org/10.1016/j.catcom.2013.11.017.

[54] C. Thomas, On an additional promoting role of hydrogen in the H_2-assisted C_3H_6-SCR of NO_x on Ag/Al_2O_3: a lowering of the temperature of formation–decomposition of the organo-NO_x intermediates? Appl. Catal. B Environ. 162 (2015) 454–462, https://doi.org/10.1016/j.apcatb.2014.07.021.

[55] C. Petitto, H.P. Mutin, G. Delahay, Hydrothermal activation of silver supported alumina catalysts prepared by sol–gel method: application to the selective catalytic reduction (SCR) of NO_x by *n*-decane, Appl. Catal. B Environ. 134 (2013) 258–264, https://doi.org/10.1016/j.apcatb.2013.01.018.

[56] F. Klingstedt, K. Eränen, L.-E. Lindfors, S. Andersson, L. Cider, C. Landberg, E. Jobson, L. Eriksson, T. Ilkenhans, D. Webster, A highly active Ag/alumina catalytic converter for continuous HC-SCR during lean-burn conditions: from laboratory to full-scale vehicle tests, Top. Catal. 30 (2004) 27–30, https://doi.org/10.1023/B:TOCA.0000029723.05170.d2.

[57] J. Wang, R. You, K. Qian, Y. Pan, J. Yang, W. Huang, Effect of the modification of alumina supports with chloride on the structure and catalytic performance of Ag/Al_2O_3 catalysts for the selective catalytic reduction of NO_x with propene and H_2/propene, Chin. J. Catal. 42 (2021) 2242–2253, https://doi.org/10.1016/S1872-2067(21)63904-9.

[58] J. So, S.J. Lee, M. Kim, H. Shin, W.B. Bae, S.B. Kang, Y.J. Kim, Steering the structure and reactivity of Ag/Al_2O_3 by the addition of multi-functional WO_x for NO_x reduction by ethanol, Appl. Catal. B Environ. 330 (2023) 122527, https://doi.org/10.1016/j.apcatb.2023.122527.

[59] J. Blanchard, R.P. Doherty, H.-Y. Law, C. Méthivier, C. Thomas, On the detrimental effect of tungstates on the *n*-C_{10}-SCR of NO_x on Ag/γ-Al_2O_3, Top. Catal. 56 (2013) 134–139, https://doi.org/10.1007/s11244-013-9942-3.

[60] R. Zhang, S. Kaliaguine, Lean reduction of NO by C_3H_6 over Ag/alumina derived from Al_2O_3, AlOOH and $Al(OH)_3$, Appl. Catal. B Environ. 78 (2008) 275–287, https://doi.org/10.1016/j.apcatb.2007.09.018.

[61] H. Deng, Y. Yu, H. He, Discerning the role of Ag–O–Al entities on Ag/γ-Al_2O_3 surface in NO_x selective reduction by ethanol, J. Phys. Chem. C 119 (2015) 3132–3142,, https://doi.org/10.1021/jp5114416.

[62] D. Mrabet, M.-H. Vu, S. Kaliaguine, T.-O. Do, A new route to the shape-controlled synthesis of nano-sized γ-alumina and Ag/γ-alumina for selective catalytic

reduction of NO in the presence of propene, J. Colloid Interface Sci. 485 (2017) 144–151, https://doi.org/10.1016/j.jcis.2016.09.021.
[63] F. Wang, J. Ma, S. Xin, Q. Wang, J. Xu, C. Zhang, H. He, X. Cheng Zeng, Resolving the puzzle of single-atom silver dispersion on nanosized γ-Al_2O_3 surface for high catalytic performance, Nat. Commun. 11 (2020) 529, https://doi.org/10.1038/s41467-019-13937-1.
[64] X. Yang, A. Wang, J. Guo, Y. Guo, Y. Guo, L. Wang, W. Zhan, γ-Al_2O_3 supported silver nanoparticle applied in C_3H_8-SCR: Nanosphere and nanoflake, Catal. Commun. 176 (2023) 106634, https://doi.org/10.1016/j.catcom.2023.106634.
[65] R. Burch, E. Halpin, J. Sullivan, A comparison of the selective catalytic reduction of NO_x over Al_2O_3 and sulphated Al_2O_3 using CH_3OH and C_3H_8 as reductants, Appl. Catal. B Environ. 17 (1998) 115–129, https://doi.org/10.1016/S0926-3373(98)00005-8.
[66] C. Petitto, G. Delahay, A new way for silver alumina catalyst preparation, Catal. Lett. 142 (2012) 433–438, https://doi.org/10.1007/s10562-012-0784-6.
[67] C. Liu, R. Li, F. Wang, K. Li, Y. Fan, R. Mu, Q. Fu, Water promoted structural evolution of Ag nanocatalysts supported on alumina, Nano Res. (2023) 9107–9115, https://doi.org/10.1007/s12274-023-5735-6.
[68] Y. Fan, F. Wang, R. Li, C. Liu, Q. Fu, Surface hydroxyl-determined migration and anchoring of silver on alumina in oxidative redispersion, ACS Catal. 13 (2023) 2277–2285, https://doi.org/10.1021/acscatal.2c05453.
[69] U. Kamolphop, S.F. Taylor, J.P. Breen, R. Burch, J.J. Delgado, S. Chansai, C. Hardacre, S. Hengrasmee, S.L. James, Low-temperature selective catalytic reduction (SCR) of NO_x with *n*-octane using solvent-free mechanochemically prepared Ag/Al_2O_3 catalysts, ACS Catal. 1 (2011) 1257–1262,, https://doi.org/10.1021/cs200326m.
[70] H. Deng, Y. Yu, H. He, Water effect on preparation of Ag/Al_2O_3 catalyst for reduction of NO_x by ethanol, J. Phys. Chem. C 120 (2016) 24294–24301, https://doi.org/10.1021/acs.jpcc.6b08886.
[71] K. Ralphs, S. Chansai, C. Hardacre, R. Burch, S.F. Taylor, S.L. James, Mechanochemical preparation of Ag catalysts for the *n*-octane-SCR de-NO_x reaction: structural and reactivity effects, Catal. Today 246 (2015) 198–206, https://doi.org/10.1016/j.cattod.2014.10.027.
[72] T. Chaieb, L. Delannoy, C. Louis, C. Thomas, Promoting Ag/Al_2O_3 performance in low-temperature H_2-C_3H_6-SCR by thermal pretreatment of γ-alumina in water, Catal. Lett. 146 (2016) 2622–2629, https://doi.org/10.1007/s10562-016-1864-9.
[73] R.M. Mironenko, O.B. Belskaya, V.P. Talsi, T.I. Gulyaeva, M.O. Kazakov, A. I. Nizovskii, A.V. Kalinkin, V.I. Bukhtiyarov, A.V. Lavrenov, V.A. Likholobov, Effect of γ-Al_2O_3 hydrothermal treatment on the formation and properties of platinum sites in Pt/γ-Al_2O_3 catalysts, Appl. Catal. A Gen. 469 (2014) 472–482, https://doi.org/10.1016/j.apcata.2013.10.027.
[74] Y. Choi, G. Kim, J. Kim, S. Lee, J.-C. Kim, R. Ryoo, H. Lee, Anchoring catalytically active species on alumina via surface hydroxyl group for durable surface reaction, Appl. Catal. B Environ. 325 (2023) 122325, https://doi.org/10.1016/j.apcatb.2022.122325.
[75] H. Kubota, S. Mine, T. Toyao, Z. Maeno, K.-i Shimizu, Redox-driven reversible structural evolution of isolated silver atoms anchored to specific sites on γ-Al_2O_3, ACS Catal. 12 (2022) 544–559, https://doi.org/10.1021/acscatal.1c04924.
[76] H. Kubota, S. Mine, T. Toyao, K.-i Shimizu, Regeneration of atomic Ag sites over commercial γ-aluminas by oxidative dispersion of Ag metal particles, Catal. Sci. Technol. 13 (2023) 1459–1469, https://doi.org/10.1039/D2CY01950G.
[77] Z.-M. Wang, M. Yamaguchi, I. Goto, M. Kumagai, Characterization of Ag/Al_2O_3 de-NO_x catalysts by probing surface acidity and basicity of the supporting substrate, Phys. Chem. Chem. Phys. 2 (2000) 3007–3015, https://doi.org/10.1039/B000226G.
[78] M. Taoufik, K.C. Szeto, N. Merle, I.D. Rosal, L. Maron, J. Trébosc, G. Tricot, R. M. Gauvin, L. Delevoye, Heteronuclear NMR spectroscopy as a surface-selective technique: a unique look at the hydroxyl groups of γ-alumina, Chem. Eur. J. 20 (2014) 4038–4046, https://doi.org/10.1002/chem.201304883.
[79] K.C. Szeto, N. Merle, J. Trébosc, M. Taoufik, R.M. Gauvin, F. Pourpoint, L. Delevoye, Caveat on the actual robustness of heteronuclear NMR methods for probing the surface of γ-alumina and related catalysts, J. Phys. Chem. C 123 (2019) 12919–12927, https://doi.org/10.1021/acs.jpcc.9b02634.
[80] N. Merle, T. Tabassum, S.L. Scott, A. Motta, K. Szeto, M. Taoufik, R.M. Gauvin, L. Delevoye, High-Field NMR, reactivity, and DFT modeling reveal the γ-Al_2O_3 surface hydroxyl network, Angew. Chem. Int. Ed. 134 (2022) e202207316, https://doi.org/10.1002/anie.202207316.
[81] A.T. Batista, T. Pigeon, J. Meyet, D. Wisser, M. Rivallan, D. Gajan, L. Catita, F. Diehl, A.-S. Gay, C. Chizallet, A. Lesage, P. Raybaud, Structure, location, and spatial proximities of hydroxyls on γ-alumina crystallites by high-resolution solid-state NMR and DFT modeling: why edges hold the key, ACS Catal. 13 (2023) 6536–6548, https://doi.org/10.1021/acscatal.3c00495.
[82] L.A. Volker, J. Meyet, Z.J. Berkson, L. Rochlitz, J.A. van Bokhoven, C. Copéret, Revisiting edge sites of γ-Al_2O_3 using needle-shaped nanocrystals and recoupling-time-encoded {27Al}-1H D-HMQC NMR spectroscopy, J. Phys. Chem. C 126 (2022) 6351–6360, https://doi.org/10.1021/acs.jpcc.2c00979.
[83] G. Lefevre, M. Duc, P. Lepeut, R. Caplain, M. Fédoroff, Hydration of γ-alumina in water and its effects on surface reactivity, Langmuir 18 (2002) 7530–7537,, https://doi.org/10.1021/la025651i.
[84] J. Abi Aad, S. Casale, M. Michau, P. Courty, F. Diehl, E. Marceau, X. Carrier, Chemical weathering of alumina in aqueous suspension at ambient pressure: a mechanistic study, ChemCatChem 9 (2017) 2186–2194, https://doi.org/10.1002/cctc.201700145.
[85] G. Busca, The surface of transitional aluminas: a critical review, Catal. Today 226 (2014) 2–13, https://doi.org/10.1016/j.cattod.2013.08.003.
[86] H. Knözinger, P. Ratnasamy, Catalytic aluminas: surface models and characterization of surface sites, Catal. Rev. Sci. Eng. 17 (1978) 31–70, https://doi.org/10.1080/03602457808080878.
[87] M. Digne, P. Sautet, P. Raybaud, P. Euzen, H. Toulhoat, Hydroxyl groups on γ-alumina surfaces: a DFT study, J. Catal. 211 (2002) 1–5, https://doi.org/10.1006/jcat.2002.3741.
[88] M. Digne, P. Sautet, P. Raybaud, P. Euzen, H. Toulhoat, Use of DFT to achieve a rational understanding of acid–basic properties of γ-alumina surfaces, J. Catal. 226 (2004) 54–68, https://doi.org/10.1016/j.jcat.2004.04.020.
[89] N.S. Barrow, A. Scullard, N. Collis, Surface selective 1H and 27Al MAS NMR observations of strontium oxide doped γ-alumina, Johns. Matthey Technol. Rev. 60 (2016) 90–97, https://doi.org/10.1595/205651316X690943.
[90] X. Zhang, Y. Yu, H. He, Effect of hydrogen on reaction intermediates in the selective catalytic reduction of NO_x by C_3H_6, Appl. Catal. B Environ. 76 (2007) 241–247, https://doi.org/10.1016/j.apcatb.2007.05.032.
[91] T. Venkov, K. Hadjiivanov, D. Klissurski, IR spectroscopy study of NO adsorption and NO+ O_2 co-adsorption on Al_2O_3, Phys. Chem. Chem. Phys. 4 (2002) 2443–2448,, https://doi.org/10.1039/B111396H.
[92] C. Pazé, G. Gubitosa, S.O. Giacone, G. Spoto, F. Llabrés i Xamena, A. Zecchina, An XRD, FTIR and TPD investigation of NO_2 surface adsorption sites of δ, γ Al_2O_3 and barium supported δ, γ Al_2O_3, Top. Catal. 30 (2004) 169–175, https://doi.org/10.1023/B:TOCA.0000029746.65404.55.
[93] J. Szanyi, J.H. Kwak, R.J. Chimentao, C.H. Peden, Effect of H_2O on the adsorption of NO_2 on γ-Al_2O_3: an in situ FTIR/MS study, J. Phys. Chem. C 111 (2007) 2661–2669,, https://doi.org/10.1021/jp066326x.
[94] M.M. Kantcheva, V.P. Bushev, K.I. Hadjiivanov, Nitrogen dioxide adsorption on deuteroxylated titania (anatase), J. Chem. Soc. Faraday Trans. 88 (1992) 3087–3089, https://doi.org/10.1039/FT9928803087.
[95] H. He, C. Zhang, Y. Yu, A comparative study of Ag/Al_2O_3 and Cu/Al_2O_3 catalysts for the selective catalytic reduction of NO by C_3H_6, Catal. Today 90 (2004) 191–197, https://doi.org/10.1016/j.cattod.2004.04.026.
[96] Z. Li, F. Wang, F. Liu, S. Xie, C. Zhang, P. Ning, K. Li, H. He, X.C. Zeng, Catalytic oxidation of ammonia: a pre-occupied-anchoring-site strategy for enlarging Ag nanoparticles at low Ag loading and achieving enhanced activity and selectivity on Ag-CuO_x/Al_2O_3 catalyst, Appl. Catal. B Environ. (2024) 123655, https://doi.org/10.1016/j.apcatb.2023.123655.